Probing the Chemical Space of Guanidino-Carboxylic Acids to Identify the First Blockers of the Creatine-Transporter-1[S]

Clemens V. Farr, Yi Xiao, Ali El-Kasaby, Manuel Schupp, Matej Hotka, Giovanni di Mauro, Amy Clarke, Miryam Pastor Fernandez, ⓘWalter Sandtner, ⓘThomas Stockner, Christoph Klade, Nuno Maulide, and ⓘMichael Freissmuth

Institute of Pharmacology and the Gaston H. Glock Research Laboratories for Exploratory Drug Development, Center of Physiology and Pharmacology, Medical University of Vienna, Vienna, Austria (C.V.F., A.E-K., M.H., A.C., W.S., T.S., M.F.); Institute of Organic Chemistry, University of Vienna, Vienna, Austria (Y.X., M.S., G.dM., M.P.F., N.M.); CeMM Research Center for Molecular Medicine of the Austrian Academy of Sciences, Vienna, Austria (Y.X., M.S., N.M.); AOP Orphan Pharmaceuticals GmbH, Vienna, Austria (C.K.); Christian Doppler Laboratory for Entropy-Oriented Drug Design, Institute of Organic Chemistry, University of Vienna, Vienna, Austria (N.M.); and NeGeMac Research Platform for Next Generation Macrocycles, Vienna, Austria (N.M.)

Received July 25, 2024; accepted September 12, 2024

ABSTRACT

The creatine transporter-1 (CRT-1/SLC6A8) maintains the uphill transport of creatine into cells against a steep concentration gradient. Cellular creatine accumulation is required to support the ATP-buffering by phosphocreatine. More than 60 compounds have been explored in the past for their ability to inhibit cellular creatine uptake, but the number of active compounds is very limited. Here, we show that all currently known inhibitors are full alternative substrates. We analyzed their structure–activity relationship for inhibition of CRT-1 to guide a rational approach to the synthesis of novel creatine transporter ligands. Measurements of both inhibition of [³H]creatine uptake and transport associated currents allowed for differentiating between full and partial substrates and true inhibitors. This combined approach led to a refined understanding of the structural requirements for binding to CRT-1, which translated into the identification of three novel compounds - i.e., compound 1 (2-(*N*-benzylcarbamimidamido)acetic acid), MIPA572 (=carbamimidoylphenylalanine), and MIPA573 (=carbamimidoyltryptophane) that blocked CRT-1 transport, albeit with low affinity. In addition, we found two new alternative full substrates, namely MIPA574 (carbamimidoylalanine) and GiDi1257 (1-carbamimidoylazetidine-3-carboxylic acid), which was superior in affinity to all known CTR-1 ligands, and one partial substrate, namely GiDi1254 (1-carbamimidoylpiperidine-4-carboxylic acid).

SIGNIFICANCE STATEMENT

The creatine transporter-1 (CRT-1) is required to maintain intracellular creatine levels. Inhibition of CRT-1 has been recently proposed as a therapeutic strategy for cancer, but pharmacological tools are scarce. In fact, all available inhibitors are alternative substrates. We tested existing and newly synthesized guanidinocarboxylic acids for CRT-1 inhibition and identified three blockers, one partial and two full substrates of CRT-1. Our results support a refined structural understanding of ligand binding to CRT-1 and provide a proof-of-principle for blockage of CRT-1.

Introduction

Lipid membranes act as barriers to the diffusion of solvated molecules. Membrane transport proteins of the solute carrier (SLC) superfamily bind these solutes as their substrates and translocate them across the cell surface and organellar membranes. Thus, solute carriers play a pivotal role in preserving cellular homeostasis. Accordingly, mutations in members of the SLC group play causative or modifying roles in human diseases (Bhat et al., 2021). Conversely, SLC transporters represent promising drug targets for therapeutic interventions (Wang et al., 2020; Casiraghi et al., 2021). Pharmacological tools are also indispensable for interrogating the physiological role of transporters and their conformational cycle. This is illustrated by the monoamine transporters, i.e., the transporters for norepinephrine, dopamine- (DAT/SLC6A3), and serotonin (SERT/SLC6A4): they are the most extensively studied solute carriers (César-Razquin et al., 2015). This is, in part, due to their medical

ABBREVIATIONS: ATPCA, 2-amino-1,4,5,6-tetrahydropyrimidine-5-carboxylic acid; CRT-1, creatine transporter-1; DAT, dopamine transporter; FDNB, 1-fluoro-2,4-dinitrobenzene; GAA, guanidinoacetate; GBA, guanidinobutyrate; GPA, guanidinopropionate; HEK293, human embryonic kidney 293 cell; NET, norepinephrine transporter; SERT, serotonin transporter; SLC, solute carrier.

relevance as targets of therapeutic and illicit drugs. Accordingly, diverse chemotypes have been identified as ligands: the resulting rich pharmacology (Sitte and Freissmuth, 2015) comprises typical inhibitors, which bind to the outward facing state, atypical inhibitors, which trap transporters in the inward facing state and which act as noncompetitive or uncompetitive inhibitors (Jacobs et al., 2007; Bulling et al., 2012; Bhat et al., 2023), allosteric modulators (Niello et al., 2020), and full and partial substrates, which can switch monoamine transporters into the exchange mode and thereby act as full and partial releasers of endogenous neurotransmitters (Bhat et al., 2019; Hasenhuetl et al., 2019).

In contrast to monoamine transporters, glucose transporters, and a few ion transporters, the vast majority of solute carriers are understudied (César-Razquin et al., 2015). In many instances, progress in defining their physiological role is hampered by the lack of high-affinity inhibitors. This is also true for the creatine transporter-1(CRT-1/SLC6A8): CRT-1 mediates the high-affinity uptake of its eponymous substrate and does so with a remarkable concentrative power (Farr et al., 2022). The intracellular accumulation of creatine to millimolar levels is necessary to supply muscle and neurons with adequate levels of phosphocreatine, which serves as an ATP-buffer (Wyss and Kaddurah-Daouk, 2000). In fact, the physiological importance of human CRT-1 is most readily evident from the phenotypic consequences of inactivating mutations in the gene encoding CRT-1. The resulting syndrome, is referred to as creatine transporter deficiency syndrome and is associated with intellectual disability, epileptic seizures, delayed speech acquisition, and autism (van de Kamp et al., 2013; Farr et al., 2020). Many of the inactivating mutations cause defective folding of CRT-1; in some instances, the folding deficiency can be restored by chemical chaperoning (El-Kasaby et al., 2019). Atypical inhibitors have been shown to rescue folding-deficient mutants of other SLC6 family members, i.e., SERT and DAT (El-Kasaby et al., 2010, 2024; Kasture et al., 2016, Beerepoot et al., 2016; Asjad et al., 2017; Bhat et al., 2017, 2021, 2023), the glycine transporter-2 (GlyT2/SLC6A5; de la Rocha-Muñoz et al., 2021), and the GABA-transporter-1 (GAT-1/SLC6A1; Kasture et al., 2023). Their binding to folding intermediates smoothens the energy landscape and promotes the completion of the folding trajectory of the mutated transporters. Thus, their pharmacochaperoning action restores export of the mutated transporter from the endoplasmic reticulum to the cell surface in functionally active form (Chiba et al., 2014; Freissmuth et al., 2018). Hence, it is justified to posit that misfolded CRT-1 variants are also amenable to pharmacochaperoning provided that (atypical) inhibitors are available. In addition, CRT-1 is expressed in many tissues other than striated muscle and neurons. In fact, it has been argued that blockage of CRT-1 is a useful strategy for targeting cancer cells, which overexpress CRT-1 (Stary and Bajda, 2023). Exploring these avenues requires inhibitors of CRT-1. However, currently, there are no CRT-1 inhibitors which arrest the transport cycle. All known inhibitors are, in fact, alternative substrates. Here, we extracted information on their structural requirements for binding to CRT-1 to search for compounds capable of blocking transport. Uptake inhibition yields reliable affinity estimates but does not allow for differentiating between alternative substrates, which are translocated and thus accumulate within cells, and true inhibitors, which

impose a conformational trap and thereby arrest the transport cycle. Accordingly, we relied on both uptake inhibition assays and electrophysiological recordings to classify existing and newly synthesized compounds. Our approach identified three compounds, which acted as transport blockers of CTR-1, albeit of low-affinity.

Materials and Methods

Materials. Human embryonic kidney 293 (HEK293) cells were bought from American Type Culture Collection (CRL-1573, Manassas, Virginia), authenticated by short tandem repeats profiling at the cell culture core facility of the Medical University of Graz, Austria, and tested on a regular basis for mycoplasma contamination by $4',6$-diamidino-2-phenylindole staining. All antibiotics were purchased from InvivoGen (San Diego, CA, USA). Penicillin–streptomycin stock solution (10.000 units/ml = 6 mg/ml penicillin and 10 mg streptomycin/ml) and Hanks's balanced salt solution were from Sigma-Aldrich. Cell culture media, salts, and buffers were obtained from Sigma-Aldrich (St. Louis, Missouri) except for $Mg(CH_3COO^-)_2$ and KH_2PO_4, which were purchased from Merck KGaA (Darmstadt, Germany). Fetal bovine serum was obtained from Capricorn Scientific (Ebsdorfergrund, Germany). The transfection reagents jetPRIME and polyethylenimine (linear 25 kDa) were purchased from Polyplus-transfection (New York City, New York) and from Santa Cruz Biotechnology (Dallas, Texas), respectively. The cDNA encoding the human creatine transporter-1/CRT-1 (transcript variant 1; SC116601) was originally bought from Origene (Rockville, Maryland) and inserted into the pEYFP-N1 vector from Clontech (Mountainview, California) to yield a version harboring YFP at the C-terminus (El-Kasaby et al., 2019). [^{3}H]Creatine (creatine [N-methyl-^{3}H], specific activity 75 Ci/mmol) and scintillation mixture (Rotiszint eco plus) were purchased from American Radiolabeled Chemicals (St. Louis, Missouri) and from Carl Roth GmbH (Karlsruhe, Germany), respectively.

Compounds were obtained from the following suppliers: creatine, cyclocreatine, 1-fluoro-2,4-dinitrobenzene (FDNB), compound **8** (=3-amino-1H-1,2,4-triazole-5-carboxylic acid), compound **9** (=2-aminobenzimidazole), compound **10** (=guanidinobenzoic acid), guanidinoacetate (GAA), guanidinobutyrate (GBA), and guanidinopropionate (GPA) were from Sigma-Aldrich St. Louis, Missouri. 2-Amino-1,4,5,6-tetrahydropyrimidine-5-carboxylic acid (ATPCA), L-arginine, L-homoarginine, compound **1** (=2-(N-benzylcarbamimidamido) acetic acid), compound **2** (=2-(2H-1,2,3-triazol-2-yl)acetic acid), compound **3** (=2-(5-amino-2H-1,2,3,4-tetrazol-2-yl)acetic acid), compound **4** (=2-(5-amino-3-methyl-1H-pyrazol-1-yl)acetic acid hydrochloride), compound **5** (=1H-1,2,4-triazole-5-carboxylic acid), compound **6** (=4-guanidinomethylbenzoic acid), compound **7** (=2-guanidino-glutaric acid = (2S)-2-carbamimidamidopentanedioic acid), and guanidinosuccinate (= (2S)-2-carbamimidamidobutanedioic acid) were from AKos Consulting and Solutions GmbH (Lörrach, Germany).

Experimental Procedures for the Synthesis of Guanidinocarboxylic Acids. Compounds for chemical synthesis were obtained from different chemical suppliers (Sigma-Aldrich, TCI Chemicals, ThermoScientific, TitolChimica, ActivateScientific, Acros Organics, Alfa Aesar) and used without further purification. Reaction progress was monitored by thin-layer chromatography (TLC) performed on aluminum plates coated with silica gel F254 with 0.2 mm thickness. Chromatograms were visualized by fluorescence quenching with ultraviolet light at 254 nm or by staining using potassium permanganate solution. Near infrared spectra were recorded using a Perkin-Elmer Spectrum 100 FT-IR spectrometer. Wavenumbers (ν_{max}) are reported in cm^{-1}. Mass spectra were obtained using a Finnigan MAT 8200 or (70 eV) or an Agilent 5973 (70 eV) spectrometer, using electrospray ionization. All ^{1}H-NMR and ^{13}C-NMR spectra were recorded using a Bruker AV-400 or AV-600 or AV 700 spectrometer at 300 K. Chemical shifts were given in parts per million (ppm, δ), referenced to the solvent peak of D_2O, defined at $\delta = 4.79$ ppm (^{1}H-NMR). Coupling constants are quoted

in Hz (J). ^{1}H-NMR splitting patterns were designated as singlet (s), doublet (d), triplet (t), and quartet (q). Splitting patterns that could not be interpreted or easily visualized were designated as multiplet (m) or broad (br).

The guanidino carboxylic acids were synthesized as racemic mixtures according to procedures reported by Jursic et al. (2000).

General Procedure A. NaOH (0.23 mol, 2.30 equiv.) was added to a solution of the corresponding amino acid (1.00 equiv. in water, 5.75 M) at room temperature, followed by a portion-wise addition of formamidinesulfinic acid (0.115 mol, 1.15 equiv.) over 30 minutes. The resulting viscous suspension was stirred at room temperature for 14 hours and subsequently heated to 60°C under continuous stirring for 30 minutes. The suspension was allowed to cool to room temperature before the crystalline product was filtered off and washed with cold methanol.

General Procedure B. NaOH (0.23 mol, 2.30 equiv.) was added to a solution of the corresponding amino acid (1.00 equiv. in water, 5.75 M) at room temperature, followed by a portion-wise addition of formamidinesulfinic acid (0.115 mol, 1.15 equiv.) over 30 minutes. The resulting viscous suspension was stirred at room temperature for 14 hours and subsequently heated to 60°C under continuous stirring for 30 minutes. The suspension was allowed to cool to room temperature. Subsequently, ethanol (3 ml) and toluene (3 ml) were added and the solvents were evaporated at ~30°C under reduced pressure. This procedure was repeated twice to remove traces of H_2O. The solid residue was slurried into methanol (10 ml) and refluxed for three hours. The solids were filtered off by hot filtration and the methanolic solution was concentrated. The product was crystallized from methanol by slow evaporation at room temperature and the crystals were separated by filtration.

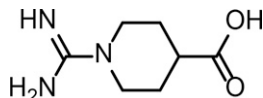**2-Guanidino-2-Methylpropanoic Acid (GiDi1253).**
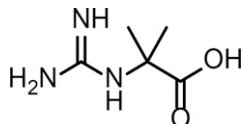
The title compound was synthesized from 2-aminoisobutyric acid (4.85 mmol) following General Procedure B and was obtained as a white solid (277 mg, 39%).

^{1}H NMR (600 MHz, D_2O) δ 1.48 (s, 6H);

^{13}C NMR (151 MHz, D_2O) δ 169.2, 151.5, 48.8, 14.5 (2C);

FTIR: ν 3042, 3028, 2939, 2843, 2802, 2613, 1636, 1303, 1576, 1542, 1470, 1459 cm^{-1}.

1-Carbamimidoylpiperidine-4-Carboxylic Acid (GiDi1254).

The title compound was synthesized from 4-piperidinecarboxylic acid (3.87 mmol) following General Procedure B and was obtained as a white solid (55 mg, 8%).
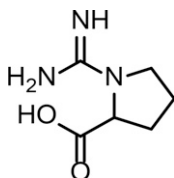
^{1}H NMR (600 MHz, D_2O) δ 3.82 (d, J = 13.6 Hz, 2H), 3.18 – 3.09 (m, 2H), 2.46 (tt, J = 11.4, 4.0 Hz, 2H), 1.95 (dd, J = 13.7, 3.2 Hz, 2H), 1.63 (ddd, J = 25.3, 11.9, 4.0 Hz, 2H);

^{13}C NMR (151 MHz, D_2O) δ 178.5, 150.9, 40.6 (2C), 38.5, 23.2 (2C);

HRMS (ESI$^+$): exact mass calculated for [M+H]$^+$ ($C_7H_{14}N_3O_2^+$) requires m/z 172.1081, found m/z 172.1081;

FTIR: ν 2962, 1545, 1491, 1366, 1088, 1013, 826, 737 cm^{-1}.

Carbamimidoylproline (GiDi1255).

The title compound was synthesized from DL-proline (4.34 mmol) following General Procedure A and was obtained as a white solid (317 mg, 46%).

^{1}H NMR (600 MHz, D_2O) δ 4.28 (dd, J = 8.6, 2.9 Hz, 1H), 3.57 (td, J = 9.0, 3.7 Hz, 1H), 3.48 (dd, J = 16.8, 8.8 Hz, 1H), 2.36 – 2.26 (m, 1H), 2.21 – 2.13 (m, 1H), 2.08 – 2.01 (m, 1H), 2.01 – 1.91 (m, 1H);

^{13}C NMR (151 MHz, D_2O) δ 168.6, 145.6, 53.2, 38.6, 21.8, 14.1;

HRMS (ESI$^+$): exact mass calculated for [M+H]$^+$ ($C_6H_{12}N_3O_2^+$) requires m/z 158.0924, found m/z 158.0924;

FTIR: ν 3219, 3063, 3041, 2995, 2363, 1681, 1587, 1310, 1299, 1272, 855, 798, 769 cm^{-1}.

1-Carbamimidoylazetidine-3-Carboxylic Acid (GiDi1257).
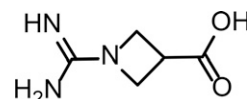
The title compound was synthesized from azetidine-3-carboxylic acid (9.59 mmol) following General Procedure B and was obtained as a white solid (400 mg, 29%).
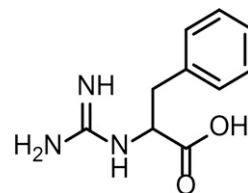
^{1}H NMR (600 MHz, D_2O) δ 4.30 (t, J = 8.9 Hz, 2H), 4.17 (dd, J = 8.5, 6.0 Hz, 2H), 3.45 (tt, J = 9.2, 6.0 Hz, 1H);

^{13}C NMR (151 MHz, D_2O) δ 177.7, 153.9, 51.2 (2C), 31.9;

HRMS (ESI$^+$): exact mass calculated for [M+H]$^+$ ($C_5H_{10}N_3O_2^+$) requires m/z 144.0768, found m/z 144.0763;

FTIR: ν 2962, 1545, 1491, 1366, 1088, 1013, 826, 737 cm^{-1}.

Carbamimidoylphenylalanine (MIPA572).

The title compound was synthesized from DL-phenylalanine (25 mmol) following General Procedure A and was obtained as a white solid (152 mg, 2.9%).

^{1}H NMR (700 MHz, D_2O) δ 7.40 (t, J = 7.4 Hz, 2H), 7.34 (t, J = 7.4 Hz, 1H), 7.31 (d, J = 7.4 Hz, 2H), 4.22 (dd, J = 8.0, 4.8 Hz, 1H), 3.27 (dd, J = 14.1, 4.7 Hz, 1H), 3.01 (dd, J = 14.1, 8.0 Hz, 1H);

^{13}C NMR (175 MHz, D_2O) δ 176.4, 156.2, 136.9, 129.3 (2C), 128.7 (2C), 127.1, 57.9, 37.8;

HRMS (ESI$^+$): exact mass calculated for [M+H]$^+$ ($C_{10}H_{14}N_3O_2^+$) requires m/z 208.1081, found m/z 208.1087;

FTIR: ν 2005, 1958, 1693, 1587, 1374, 880, 824, 723, 700 cm^{-1}.

Carbamimidoyltryptophan (MIPA573).
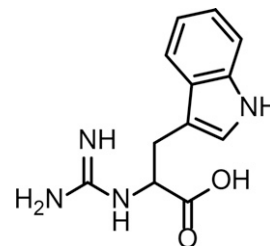
The title compound was synthesized from DL-tryptophan (25 mmol) following General Procedure A and was obtained as a white solid (531 mg, 8.8%).

^{1}H NMR (700 MHz, D_2O) δ 7.71 (d, J = 7.9 Hz, 1H), 7.53 (d, J = 8.2 Hz, 1H), 7.30 – 7.24 (m, 2H), 7.21 – 7.17 (m, 1H), 4.30 (dd, J = 7.4, 4.7 Hz, 1H), 3.45 (dd, J = 14.9, 4.6 Hz, 1H), 3.22 (dd, J = 14.9, 7.4 Hz, 1H);

^{13}C NMR (175 MHz, D_2O) δ 176.8, 156.2, 136.1, 127.1, 124.5, 121.8, 119.3, 118.5, 111.8, 109.4, 57.4, 27.7;

HRMS (ESI$^+$): exact mass calculated for [M+H]$^+$ (C$_{12}$H$_{15}$N$_4$O$_2$$^+$) requires m/z 247.1190, found m/z 247.1195;

FTIR: ν 3798, 3273, 2570, 2179, 1862, 846, 773 cm^{-1}.

Carbamimidoylalanine (MIPA574).

The title compound was synthesized from DL-alanine (25 mmol) following General Procedure A and was obtained as a white solid (139 mg, 3.6%).

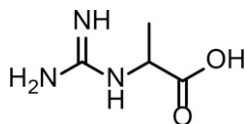^{1}H NMR (700 MHz, D$_2$O) δ 3.99 (q, J = 7.1 Hz, 1H), 1.43 (d, J = 7.1 Hz, 3H);

^{13}C NMR (175 MHz, D$_2$O) δ 178.5, 156.2, 52.3, 17.8;

HRMS (ESI$^+$): exact mass calculated for [M+Na]$^+$ (C$_4$H$_9$N$_3$O$_2$Na$^+$) requires m/z 154.0587, found m/z 154.0590;

FTIR: ν 3919, 3127, 2272, 2188, 1952, 1129, 863, 621, 604 cm^{-1}.

Cell Culture and Transfections of HEK293 Cells. HEK293 cells were purchased from ATCC (CRL-1573, ATCC, Manassas, VA, USA; RRID:CVCL_0045). HEK293 cells were cultured in Dulbecco's modified Eagle's medium containing high glucose (4.5 g/L = 25 mM), L-glutamine (584 mg/L = 4 mM), 10% fetal bovine serum, 0.6 g/L penicillin and 0.1 g/L streptomycin in a humidified atmosphere containing 5% CO$_2$ at 37°C. For electrophysiological recordings, cells were split every 2–4 days to maintain subconfluent cultures (confluency < 50%). The cells were transiently transfected with a plasmid encoding C-terminally YFP-tagged human CRT-1 with jetPRIME (3 μg DNA/6 cm dish) and polyethylenimine (20 μg DNA/15 cm dish) for patch clamp experiments and for uptake experiments according to the manufacturer's protocol, respectively. These ratios gave comparable transfection efficiency. One day after the transfection, cells were seeded at low density onto 3.5 cm dishes precoated with poly-D-lysine for electrophysiological measurements. Similarly, 24 hours after transfection, cells were seeded onto 96-well (36.000 cells/well) plates for uptake inhibition experiments.

Cell Culture and Transfection of Hippocampal Neurons. Pregnant Sprague-Dawley rats were provided by the Department of Biomedical Research, Division for Laboratory Animal Science and Genetics, Himberg, Austria. Neonatal animals were killed by decapitation in full accordance with all rules of the Austrian animal protection law (see http://www.ris.bka.gv.at/Dokumente/BgblAuth/BGBLA_2012_I_114/BGBLA_2012_I_114.pdf) and the Austrian animal experiment by-laws (see http://www.ris.bka.gv.at/Dokumente/BgblAuth/BGBLA_2012_II_522/BGBLA_2012_II_522.pdf) which implement European (DIRECTIVE 2010/63/EU; see http://eurlex.europa.eu/LexUriServ/LexUriServ.do?uri=OJ:L:2010:276:0033:0079:en:PDF) into Austrian law (all information accessed on August 30th, 2019). The responsible animal welfare body is the Ethics Committee of the Medical University of Vienna for Research Projects Involving Animals. Brains were removed to dissect the hippocampi in ice-cold buffer. Primary cocultures of hippocampal neurons and glial cells were prepared after enzymatic digestion of the tissue with papain and mechanical dissociation with Pasteur pipettes (trituration) as described previously (Hotka et al., 2020). Neurons were cultured for at least 12 days at 37°C and 5% CO$_2$ in DMEM-high glucose (20 mm glucose; D5796, Sigma-Aldrich) supplemented with 10% gamma-irradiated fetal bovine serum (catalog #S 0415, Biochrom). Transfections of neurons were performed using Lipofectamine 2000 reagent (Invitrogen, Thermo Fisher Scientific) according to the manufacturer's instructions with some modifications. In brief, neuronal cultures older than 12 days-in-vitro (DIV) were incubated in 0.5 ml of antibiotic-free medium containing 3 μl of Lipofectamine and 1 μg of plasmid DNA for 3 hours. The transfection medium was replaced with original medium and the neurons were kept for 3 days in the incubator. Experiments were performed on day 3 after transfection.

Uptake Inhibition. Twenty-four hours after seeding, HEK293 cells were washed twice with Hank's balanced salt solution and incubated therein for 30 minutes at 37°C and under 5% CO$_2$. Subsequently, the solution was replaced by Krebs-HEPES buffer (10 mM HEPES. NaOH, 4.7 mM KCl, 2.2 mM CaCl$_2$, 1.2 mM MgSO$_4$, 10 mM glucose, 120 mM NaCl, pH = 7.4). In uptake inhibition experiments, logarithmically spaced concentrations of competing substrates were added, the reaction was initiated by adding [^{3}H]creatine (1 μM, specific activity adjusted to 0.75 Ci/mmol with unlabeled creatine) and allowed to proceed for 6 minutes at 37°C. Nonspecific uptake was defined in the presence of 300 μM β-GPA. Assays were done in triplicate. The uptake reaction was terminated by aspiration of the solution and two rapid washes with ice cold Krebs-HEPES buffer. Cells were lysed in 1% SDS, the lysates were transferred to scintillation vials and the radioactivity content was determined by liquid scintillation counting. Assays were done in triplicate.

Electrophysiology. Sixteen to 24 hours after seeding, currents were recorded from single HEK293 cells in the whole-cell patch clamp configuration at 20–24 °C. Cells were maintained in an aqueous external buffer (standard external solution) composed of 140 mM NaCl, 2.5 mM CaCl$_2$, 2 mM MgCl$_2$, 20 mM glucose and 10 mM HEPES (pH adjusted with NaOH to pH 7.4). The internal solution in the micropipette contained 5.9 mM NaCl, 1 mM CaCl$_2$, 0.7 mM MgCl$_2$, 10 mM EGTA, 10 mM HEPES, and 133 mM K-gluconate (pH adjusted with KOH to pH 7.2). The composition of the solutions given in the figures reflect the ionic concentrations after pH adjustment. Compounds and solutions were applied using an Octaflow II system (ALA Scientific Instruments, Farmingdale, New York) and a Quartz Micromanifold (eight tubes with an inner diameter of 100 μM for application and a ninth tube with an inner diameter of 200 μm for flushing; fluorinated ethylene-propylene tubings) (ALA Scientific Instruments, Inc., Farmingdale, New York). Currents were recorded via an Axopatch 200B amplifier (MDS Analytical Technologies, Sunnyvale, California) coupled with pClamp 10.2 software (Molecular Devices, LLC, San José, California) and digitized at 10 kHz using a Digidata 1440 A data acquisition system (MDS Analytical Technologies). Recordings were filtered at 100 Hz and analyzed with Clampfit 10.2 software (Molecular Devices, LLC).

Imaging. Experiments were done as previously described (Hotka et al., 2020): in brief, neurons and glial cells were cocultured in glass bottom dishes (P35GC-1.5-14-C, MatTek Corporation). Before each experiment, the culturing medium was replaced by external solution containing 140 mM NaCl, 3 mM KCl, 2 mM CaCl$_2$, 2 mM MgCl$_2$, 10 mM HEPES, and 20 mM glucose (pH was adjusted to 7.4 by NaOH). Experiments were performed at room temperature; cells were superfused continuously using an 8-reservoir drug application system (Octaflow II) with a micromanifold with eight channels converging into a 100 μM diameter quartz outlet. Neurons were imaged using a Nikon A1R confocal microscope equipped with a focus clamp. The ATP/ADP ratio was determined in neurons expressing the genetically encoded fluorescence sensor PercevalHR, with excitation at 403 nm and 488 nm and the emission recorded at 525 nm. A region of interest was defined over the neuronal somata and the fluorescence intensity recorded over this area was averaged. The quotient F488/F403 reflects the intraneuronal ATP/ADP ratio. The expression vector GW1-PercevalHR was a gift from Gary Yellen (Addgene plasmid # 49082) (Tantama et al., 2013).

Ligand Docking. PDB files for the ligands were built using the Maestro 3D Builder tool. For the compounds MIPA574, MIPA572, and MIPA573, two enantiomeric forms exist, and PDB files were built for both. The homology model of CRT-1 from Clarke et al. (2024) was then used for docking the ligands. Following the docking protocol from Clarke et al. (2024), the HADDOCK v2.4 webserver was used (first accessed on 09/10/2023) (Honorato et al., 2021; van Zundert et al., 2016). In all docking runs, the Cl$^-$ and Na$^+$ cosubstrate ions were present, and the truncated protein (residues 46 to 603) was used. All parameters were kept as the default HADDOCK run parameters. Subsequent to the HADDOCK docking, the best models of the top five clusters were selected for further analysis. For these models, the distance between NA1 of CRT-1 and the carbon atom of the carboxylic acid moiety of the ligand was calculated. In Clarke et al. (2024), the distance

between these two atoms did not exceed 0.6 nm. Consequently, any docked models where the distance between these two atoms exceeded 0.6 nm was discarded. Of the remaining models, the model with the highest score according to the HADDOCK scoring function was selected as the top pose. Visualization of the docked pose used the Maestro Ligand Interaction Diagram (two-dimensional diagrams) and UCSF Chimera (three-dimensional diagrams).

Data Analysis and Statistics. Uptake assays were done in triplicate, which were averaged to obtain data points (i.e., experimental means in individual assays), and were reproduced three to four times in independent experiments. These data points from these individual assays were used to calculate means ± S.D. Data from saturation and inhibition uptake experiments were fitted by curvilinear regression to the equation for a rectangular hyperbola using GraphPad Prism 6 (Graphpad Software, San Diego, California) or Sigma Plot 12.0 (Systat Software, Inc. (San Jose, California). The statistical comparison of current amplitudes and of fluorescence intensities was done by paired t test and by Wilcoxon signed rank test for data, which followed and did not follow a normal distribution, respectively.

Results

Structural Requirements for Inhibition of Substrate Uptake by CRT-1. We searched the published literature for compounds, which had been tested as inhibitors of creatine uptake by (mammalian) tissues or by cells, which heterologously expressed CRT-1: this survey identified 65 compounds, which had been previously analyzed. Of these, 13 (shown in Fig. 1 and Supplemental Fig. 1) were reported to convey inhibition of creatine uptake (the references to the relevant studies can be found in Supplemental Tables 1 and 2): all inhibitors – but ATPCA II and taurocyamine – harbored both the guanidino and the carboxyl group present in creatine, separated by one to three carbon atoms. In our first round of screening, we selected commercially available compounds with structural similarity to creatine to further probe the importance of the guanidino group and/or the carboxylate (structures shown in Fig. 1A). We first measured the uptake of [³H]creatine into HEK293 cells transiently transfected with CRT-1 in the presence of a high concentration (i.e., 1 mM) of these commercially available substances. As controls, we included known CRT-1 inhibitors (i.e., GAA, GPA, GBA, ATPCA, and cyclocreatine) and endogenous guanidinocarboxylic acids, which are either known (i.e., guanidinosuccinate and arginine) or suspected (i.e., homoarginine; Lygate et al., 2022) not to inhibit CRT-1. At 1 mM, unlabeled creatine completely inhibited [³H]creatine uptake as did the positive controls GPA, ATPCA, and cyclocreatine (Fig. 1B). As expected, compounds containing only one of the two pertinent functional groups (i.e., compounds **2** and **9**) failed to inhibit CRT-1-mediated creatine uptake. Among the other guanidinocarboxylic acids, only compound **1** led to inhibition (36.43 ± 3.84% of control uptake). The structures of GAA and GBA differ only modestly from that of creatine and GPA (Supplemental Fig. 1). However, at 1 mM both GAA and GBA did not fully inhibit [³H]creatine uptake (Fig. 1B). In addition, there is large variation in the reported affinity of GAA (see Table 1). Accordingly, we generated concentration-response curves for compound **1**, GPA (as a reference), compound **10** (as negative control), GAA, and GBA (Fig. 1C). Except for compound **10**, the concentration-dependent inhibition of [H³]creatine uptake was adequately described by a monophasic inhibition curve. The inhibition constant (K_i) of compound

1 was 407.8 ± 52.1 μM (Table 1). The K_i of GPA (15.7 ± 1.4 μM) was in the range previously reported (Table 1). The K_i values of GAA (106.7 ± 14.8 μM) and GBA (108.4 ± 18.8 μM) were essentially identical and were lower than determined in earlier experiments (Table 1). GAA, GPA, and GBA differ only by the length of the alkyl chain separating the guanidino and the carboxyl group. The fact that GAA and GBA are substantially less potent than GPA indicates that the distance between the carboxylate and the guanidino group is an important determinant of affinity. Similarly, the lower affinity of GAA than that of creatine highlights a contribution of the methyl addition to the guanidino group on creatine to its affinity. Compound **1** differs from creatine by the additional bulky phenyl-substituent, which confers a lower affinity.

Differentiating between Alternative Substrates and Blockers of CRT-1. For each molecule of creatine, CRT-1 cotransports two sodium ions and one chloride ion (Farr et al., 2022). Creatine does not carry any net charge. Therefore, one positive charge is transferred across the cell membrane during each transport cycle of CRT-1. As outlined in Fig. 2A, (co)-substrate translocation by CRT-1 therefore produces steady-state currents, which can be measured by electrophysiological recordings (Farr et al., 2022). Accordingly, we employed the patch clamp technique to study the ability of CRT-1 to translocate different compounds: we clamped the membrane voltage of HEK293-cells to -60 mV and employed physiological extra- and intracellular ion concentrations (indicated in Fig. 2A). HEK293 cells transiently expressing CRT-1 were first superfused with a saturating concentration of creatine (i.e., 500 μM) to elicit steady-state currents (representative current traces in Fig. 2B, left hand side). The absence of currents in untransfected HEK293 cells (Fig. 2B, right hand side) confirmed that creatine-elicited currents were carried by CRT-1. After washout of creatine with external solution, cells were sequentially subjected to superfusion with different compounds. Substrate-induced currents through CRT-1 are coupled to substrate translocation (Farr et al., 2022). In line with the results from Fig. 1B, compounds **2-10**, arginine, homoarginine and guanidinosuccinate did not trigger CRT-1 mediated currents at a concentration of 1 to 3 mM (data not shown). GAA, GPA, GBA, ATPCA and cyclocreatine were previously shown to be transported by CRT-1 (Tachikawa et al., 2008; Valayannopoulos et al., 2013; Al-Khawaja et al., 2018; Farr et al., 2022). However, transport rates of these substrates of CRT-1 have never been compared in a pairwise manner to the transport rate of creatine in the same individual cells. Therefore, it remained unclear if they were transported with the same maximum rates by CRT-1 as creatine, that is if they are full or partial substrates. Partial substrates are translocated at a slower rate than full substrates (Rothman et al., 2012). Current equals charge transfer over time. Therefore, amplitudes of transport-associated currents reflect the rate of transport such that, in patch-clamp recordings, partial substrates elicit smaller current amplitudes than full substrates (Sandtner et al., 2016; Bhat et al., 2017). Partial substrates offer an avenue to identifying inhibitors: there is a continuum, which extends from full over partial substrates eventually to blockers, which are accommodated in the substrate binding site but impede the conformational transition(s) required for supporting the transport cycle (Sandtner et al., 2016; Hasenhuetl et al., 2019). Accordingly, we used concentrations of
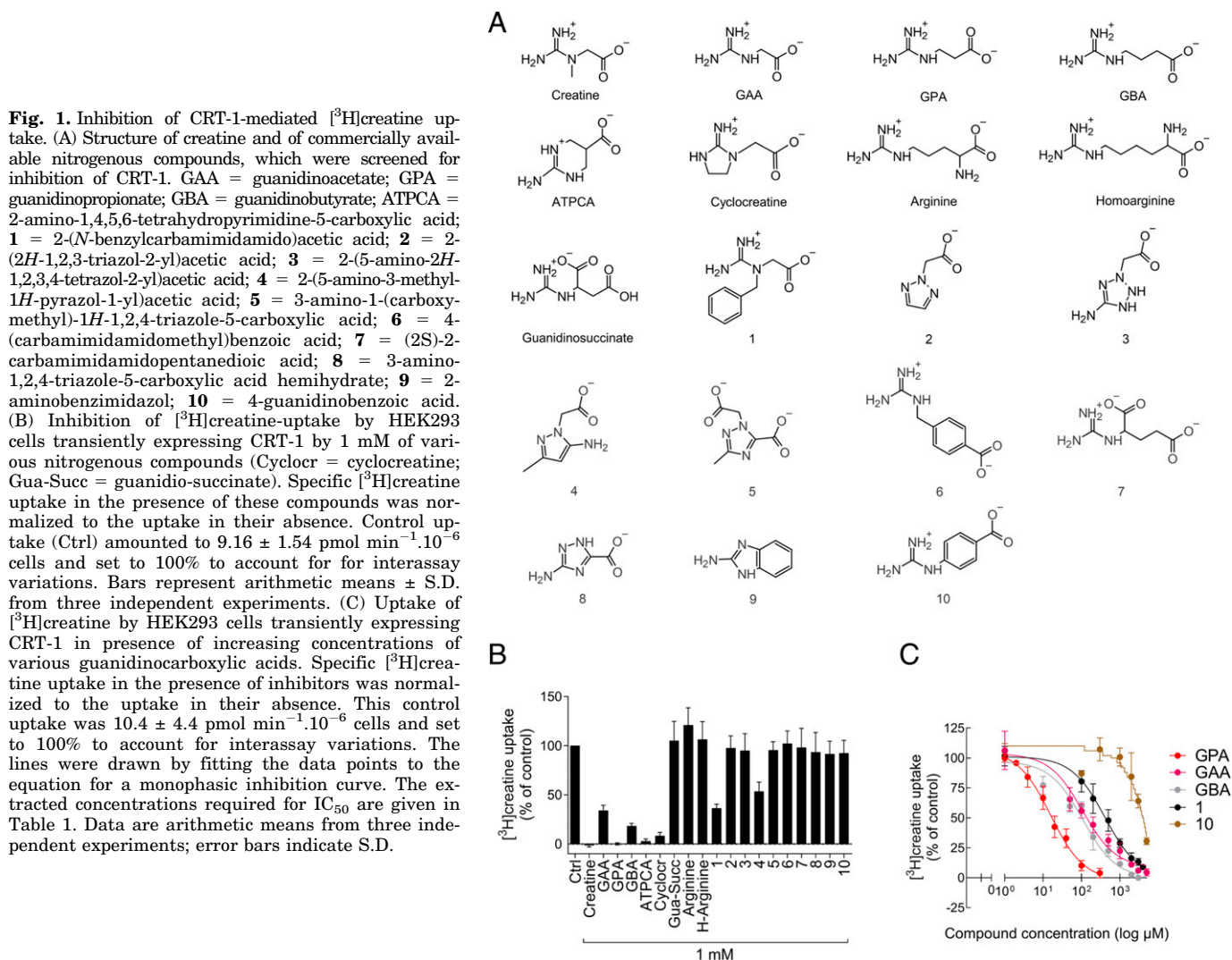
Fig. 1. Inhibition of CRT-1-mediated [³H]creatine uptake. (A) Structure of creatine and of commercially available nitrogenous compounds, which were screened for inhibition of CRT-1. GAA = guanidinoacetate; GPA = guanidinopropionate; GBA = guanidinobutyrate; ATPCA = 2-amino-1,4,5,6-tetrahydropyrimidine-5-carboxylic acid; **1** = 2-(*N*-benzylcarbamimidamido)acetic acid; **2** = 2-(2*H*-1,2,3-triazol-2-yl)acetic acid; **3** = 2-(5-amino-2*H*-1,2,3,4-tetrazol-2-yl)acetic acid; **4** = 2-(5-amino-3-methyl-1*H*-pyrazol-1-yl)acetic acid; **5** = 3-amino-1-(carboxymethyl)-1*H*-1,2,4-triazole-5-carboxylic acid; **6** = 4-(carbamimidamidomethyl)benzoic acid; **7** = (2S)-2-carbamimidamidopentanedioic acid; **8** = 3-amino-1,2,4-triazole-5-carboxylic acid hemihydrate; **9** = 2-aminobenzimidazol; **10** = 4-guanidinobenzoic acid. (B) Inhibition of [³H]creatine-uptake by HEK293 cells transiently expressing CRT-1 by 1 mM of various nitrogenous compounds (Cyclocr = cyclocreatine; Gua-Succ = guanidio-succinate). Specific [³H]creatine uptake in the presence of these compounds was normalized to the uptake in their absence. Control uptake (Ctrl) amounted to 9.16 ± 1.54 pmol min^{-1}.10^{-6} cells and set to 100% to account for for interassay variations. Bars represent arithmetic means ± S.D. from three independent experiments. (C) Uptake of [³H]creatine by HEK293 cells transiently expressing CRT-1 in presence of increasing concentrations of various guanidinocarboxylic acids. Specific [³H]creatine uptake in the presence of inhibitors was normalized to the uptake in their absence. This control uptake was 10.4 ± 4.4 pmol min^{-1}.10^{-6} cells and set to 100% to account for interassay variations. The lines were drawn by fitting the data points to the equation for a monophasic inhibition curve. The extracted concentrations required for IC$_{50}$ are given in Table 1. Data are arithmetic means from three independent experiments; error bars indicate S.D.

GAA, GPA, GBA, ATPCA, and cyclocreatine, which based on their K_i values (see Fig. 1C and Table 1), were predicted to result in >90% occupancy of CRT-1. In cells expressing CRT-1, GAA, GPA, GBA, ATPCA, and cyclocreatine triggered steady-state currents, which were comparable in magnitude to that elicited by 0.5 mM creatine (Fig. 2B, left hand side). Fig. 2C summarizes the pairwise recordings from multiple cells. Transient transfection results in variable expression levels. Hence, we observed cell-dependent variation in the amplitude of steady state currents (the amplitudes induced by creatine, GAA, GPA, GBA, ATPCA, and cyclocreatine ranged from −3.2 to −35.7 pA, −6.3 to −20.0 pA, −9.3 to −36.3 pA, −5.5 to −12.0 pA, −5.3 to −13.5 pA and −8.3 to −38.8 pA, respectively). However, a pairwise comparison by the Wilcoxon-signed rank test showed that, when recorded in the same cell, current amplitudes elicited by creatine and alternative substrates did not differ in a statistically significant manner (Fig. 2C). Thus, based on these data, we conclude that all known substrates of CRT-1 are full substrates. In contrast, compound **1** did not elicit measurable currents through CRT-1 (Fig. 2, B and C), although it was used at a concentration (3 mM), which inhibited creatine uptake by approximately 90% (cf. Fig. 1C). We stress that this compound does not carry a net charge. Therefore, its translocation by CRT-1 together with the cosubstrate ions ought to produce currents. Hence, we conclude that compound **1** is not transported by CRT-1, i.e., compound **1** is an inhibitor of CRT-1.

Rational Synthesis of Novel Guanidino-Carboxylic Acids. Compounds **6**, **10**, and ATPCA contain a 6-membered ring. The distance between the guanidine and carboxylic group in compounds **6** and **10** is larger than in ATPCA by 1 and 2 carbon atoms, respectively. In contrast to ATPCA, compounds **6** and **10** failed to inhibit CRT-1. We therefore inferred that in compounds **6** and **10**, the distance between the functional groups exceeded the upper limit required for CRT-1 binding. Notably, GBA remained a full substrate like GPA (*cf.* Fig. 2C), although the extra carbon in GBA was penalized by a 7-fold reduction in affinity (Table 1). Smaller guanidinocarboxylic acids harboring additional charges (i.e., compounds **5** and **7** and guanidinosuccinate) failed to inhibit CRT-1. Therefore, we surmised that preserving the zwitterionic character would favor binding to CRT-1. The presence of an aromatic residue in the linker region as found in compound **1** precluded translocation by CRT-1 but was penalized by a poor affinity.

We relied on a homology model of CRT-1, which is based on the structure of SERT (Clarke et al., 2024), for docking of

TABLE 1
Inhibitor constants for inhibition of CRT-1 mediated or tissue creatine uptake determined experimentally and compiled from the literature

	Experiment K_i (μM)	Literature		
		K_i (μM)	$K_{M \text{ (creatine)}}$ (μM)	Reference
GAA	106.7 ± 14.8	494	46	Dodd et al., 2010
		3000	500	Fitch et al., 1968
GPA	15.7 ± 1.4	200	500	Fitch et al., 1968
		450	21	Ku and Passow, 1980
		23 ± 4	46	Schloss et al., 1994
		22	20	Dai et al., 1999
		9	—	Al-Khawaja et al., 2018
		19 ± 1	48 ± 7	Farr et al., 2022
GBA	108.4 ± 18.8	349	20	Dai et al., 1999
Compound **1**	407.8 ± 52.1	—	—	
Cyclocreatine	—	185	20	Dai et al., 1999
		167 ± 10	48 ± 7	Farr et al., 2022
ATPCA	—	65	—	Al-Khawaja et al., 2018
		105 ± 7	48 ± 7	Farr et al., 2022
N-ethyl-GAA	—	1000	500	Fitch et al., 1968
ATPCA II	—	670	—	Al-Khawaja et al., 2018
Taurocyamine/GES	—	1377	20	Dai et al., 1999

K_i values (±S.D.) of CRT-1 mediated [³H]creatine uptake given in the second column (from left) were obtained from the experiments described in Fig. 1C. The third column from the left lists K_i values obtained from the literature (IC$_{50}$ values obtained from the literature were converted to K_i values using the Cheng-Prusoff equation). The affinity of creatine determined in the respective studies (fourth column) serve as an interassay comparator. Italic references (Fitch et al., 1968; Ku and Passow, 1980 and Dodd et al., 2010) report endogenous creatine uptake by rat skeletal muscle, erythrocytes and hippocampal neurons, respectively. In the other references (Schloss et al., 1994; Dai et al., 1999; Al-Khawaja et al., 2018; Farr et al., 2022), creatine uptake was determined in cells heterologously expressing CRT-1. ATPCA II = 6-amino-2,3,4,5-tetrahydropyridine-3-carboxylic acid hydrochloride; GES, guanidinoethane sulfate.

ligands (Fig. 3A). The docking poses of creatine indicated that creatine bound in an extended conformation (Fig. 3B). In addition, hydrophobic regions were identified in the vicinity of the substrate, e.g., in the region of A^{69}-L^{72} and of Y^{147}-Y^{148} on transmembrane (TM) helices TM1 and TM3, respectively (Fig. 3B). Docking of compound **1** into the homology model of CRT-1 indicated that the phenyl ring of compound **1** indeed engaged Y147 and Y148 by hydrophobic contacts (Fig. 4A).
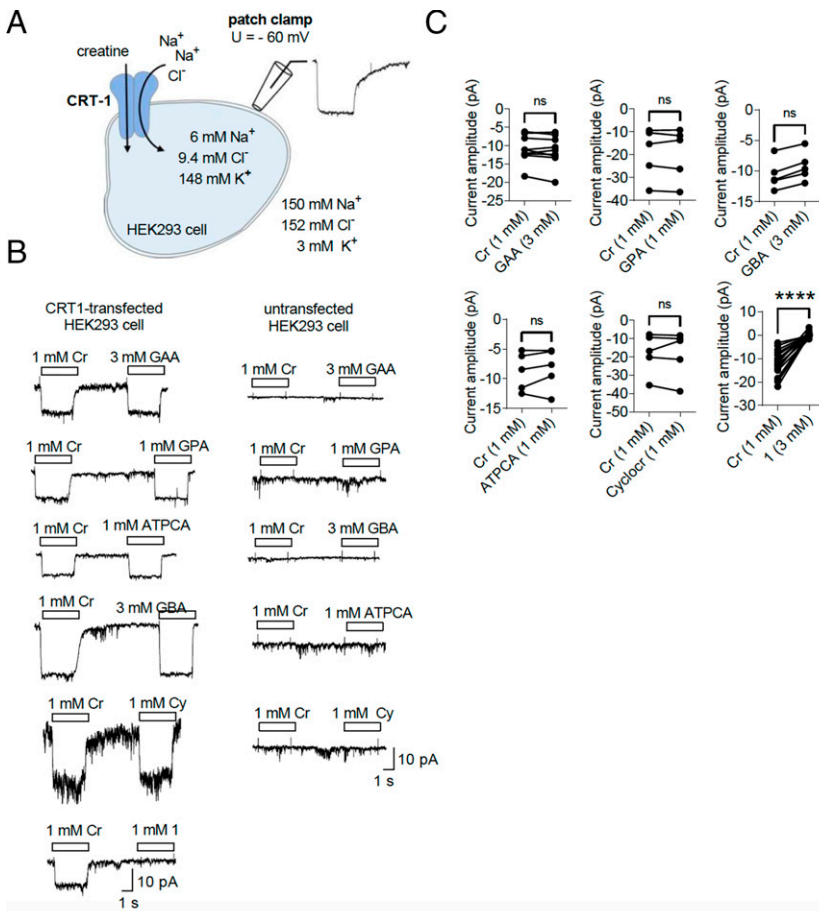

Fig. 2. Patch clamp-recordings of currents elicited by creatine and creatine analogs in HEK293 cells expressing CRT-1. (A) The schematic representation illustrates the approach to measuring transporter-associated currents: for each translocated substrate CRT-1 cotransports 1 Cl⁻ and 2 Na⁺ ions. If the substrate is electroneutral (such as creatine), this results in a net movement of one positive charge. Continuous transporter cycling thus leads to steady-state currents, which can be recorded by the patch-clamp technique. The scheme also indicates the extra- and the intracellular ion concentrations and the membrane potential used in panels (B) and (C). (B) Representative current traces measured by patch-clamping of CRT-1 expressing (left hand side) and untransfected (right hand side) HEK293 cells: cells were first superfused with a saturating concentration (1 mM) of creatine (Cr). After subsequent washout with external solution cells were then subjected to saturating concentrations of 3 mM GAA, 1 mM GPA, 1 mM ATPCA, 3 mM GBA, 1 mM cyclocreatine or 1 mM compound **1**. White boxes indicate the superfusion steps. (C) Amplitudes of steady state currents through CRT-1 elicited by GAA (n = 9; mean ± S.D.: −11.3 ± 4.1 pA), GPA (n = 5; −19.4 ± 11.5 pA), GBA (n = 9; −9.1 ± 3.3 pA), ATPCA (n = 5; −8.3 ± 3.4 pA), cyclocreatine (n = 5; −17.9 ± 12.7 pA) and compound 1 (n = 18; −0.25 ± 1.06 pA) in HEK293 cells transfected with CRT-1 at the concentrations given in (B). Amplitudes were paired to current amplitudes triggered by 1 mM creatine for each individual cell: statistically significant differences were found only for compound **1** (Wilcoxon signed rank test, $P < 0.0001$, ****).

These insights and additional considerations were taken into account for a rational approach to the synthesis of additional guanidinocarboxylic acids (Fig. 5A), which interrogated the structural determinants of substrate affinity: (i) GiDi1255 was devised to probe, if an altered angle between the functional groups impeded binding to CRT-1. (ii) GPA is the CRT-1 substrate with the highest known affinity. We prepared an azetidine derivative (GiDi1257), positing that the rigid four-membered architecture of GiDi1257 would minimize entropic penalties upon binding, which ought to accelerate adoption of the correct binding pose and therefore increase affinity (van der Kolk et al., 2022). (iii) GAA has a lower affinity than creatine. Accordingly, we also analyzed the role of the methyl group in determining affinity: MIPA574 harbors the methyl group on the carbon rather than the nitrogen. This allowed for gauging if the methyl group conveyed affinity by a positive inductive effect on the neighboring nitrogen or by entering a hydrophobic pocket in the binding site of CRT-1. GiDi1253 was used to explore if an additional methyl group translated into an affinity gain. (iv) Compound **1** was the only CRT-1 ligand which was not translocated (*cf.* Fig. 2, B and C). Compound **1** thus served as the starting point to search for additional inhibitors rather than alternative substrates of CRT-1. MIPA572 is a version of compound **1** in which the methylphenyl group was attached as steric bulk to the linker carbon rather than to the nitrogen atom. We surmised that an unsubstituted guanidino-group would favor CRT-1 binding because GPA is the substrate with the highest affinity. The rationale underlying the synthesis of MIPA573 was to examine if addition of a yet more substantial bulk was tolerated by CRT-1. (vi) Finally, we expanded the linker region per se by generating GiDi1254; we posited that this compound ought to inhibit CRT-1 because it did not exceed the suspected critical length for binding (as opposed to compounds **6** and **10**), but it carried more bulk between the functional groups than ATPCA.

Characterization of Novel Compounds. We analyzed the uptake of [^{3}H]creatine in the presence of the newly synthesized compounds and GPA was used as reference compound. Because MIPA573 had to be dissolved in DMSO, we included controls for DMSO carryover in the uptake assays shown in Fig. 5, B and C. At 1 mM, GiDi1253 and GiDi1255 failed to inhibit [^{3}H]creatine uptake (Fig. 5B). MIPA572, MIPA573, MIPA574, and GiDi1254 displayed modest inhibition, thus supporting our hypothesis that addition of neutral bulk to guanidinoacetate was tolerated to some extent by CRT-1 (Fig. 5B). GiDi1257 was the only compound leading to full inhibition of creatine uptake at a concentration of 1 mM (Fig. 5B). We generated concentration–response curves for inhibition of CRT-1 mediated [H^3]creatine uptake by the active compounds; these were adequately described by the equation for monophasic inhibition (Fig. 5C). As expected from the data in Fig. 5B, GiDi1257 was the most potent inhibitor ($K_i = 14.8 \pm 2.4$ μM). The K_i of GiDi1254 was 390 ± 93 μM, i.e., roughly four times higher than that of GBA, which was of identical length. The K_i estimated for MIPA573 ($K_{i\text{-MIPA573}} = 500 \pm 57$ μM) was similar to that of compound **1**, indicating that CRT-1 tolerated enlargement of the bulk. However, the K_i estimated for MIPA572 ($K_{i\text{-MIPA572}} = 1.19 \pm 0.01$ mM) was 2-fold higher than that of compound 1; this observation refuted the hypothesis that shifting of the aliphatic rest from the guanidine-group to the linker carbon would enhance affinity. Similarly, MIPA574, which harbored the methyl

group on the linker carbon rather than the nitrogen as in creatine, had a substantially lower affinity ($K_{i,\text{ MIPA574}} = 1.15 \pm 0.15$ mM) than creatine ($K_M = K_i = 20$ to 50 μM, cf. Table 1).

All novel compounds are zwitterions. If they are transported by CRT-1, their translocation (together with cosubstrate ions) must be electrogenic. Accordingly, we recorded the currents triggered by superfusing HEK293 cells with the newly synthesized compounds to differentiate substrates from transport blockers. None of the compounds elicited a measurable current in untransfected HEK293 cells (representative current traces are shown for MIPA574, GiDi1254 and GiDi1257 in the top row of Fig. 5D). GiDi1253 (left-hand trace in the second row of Fig. 5D) and GiDi1255 (right-hand trace in the second row of Fig. 5D) did not elicit any appreciable currents in HEK293 cells transiently expressing CRT-1. Because these compounds were inactive as inhibitors of [^{3}H]creatine uptake (*cf.* Fig. 5B), we conclude that they lack appreciable affinity for CRT-1. In contrast, MIPA574 (left-hand traces in the third row, Fig. 5D) and GiDi1257 (left-hand traces in the third row, Fig. 5D) elicited currents in CRT-1 expressing HEK293 cells, which were comparable to that seen in the presence of creatine. In fact, the pairwise comparison of creatine and either GiDi1257 or MIPA574 showed that the current amplitudes did not differ in a statistically significant manner (Fig. 5D). Thus, both, GiDi1257 and MIPA574 are full substrates, albeit of high and low affinity, respectively. Superfusion with MIPA572 and MIPA573 failed to trigger steady-state currents in CRT-1 expressing HEK293 cells (*cf.* representative traces and compiled pairwise comparison with creatine in the fourth row of Fig. 5D). Thus, these two compounds were not translocated as substrates by CRT-1, but they inhibited substrate uptake by CRT-1 (cf. Fig. 5, B and C). This demonstrates that they bind to and block CRT-1 in a manner similar to compound **1**. Taken together, the results for GiDi1257, MIPA574, MIPA572, and MIPA573 were consistent with the hypothesis that bulk is required to produce a blocker. Both compounds, GiDi1257 and MIPA574, are devoid of bulky substituents and thus substrates; conversely, MIPA572 and MIPA573 harbor bulky substituents and are CRT-1 blockers, albeit of low affinity. Superfusion of cells with 3 mM GiDi1254 also triggered currents through CRT-1. However, these currents were significantly lower than those elicited by superfusion with creatine (bottom row in Fig. 5D). At 3 mM, GiDi1254 is predicted to yield >90% occupancy of CRT-1 (Fig. 5C) and thus to be close to saturation. Because the currents were smaller than those seen with 0.5 mM creatine (i.e., at equivalent occupancy of CRT-1 by creatine), we conclude that GiDi1254 is a partial substrate of CRT-1. Thus, consistent with our hypothesis, the enhanced bulkiness of GiDi1254 (relative to that of ATPCA) impeded the conformational transition of CRT-1 required for substrate translocation. However, the trade-off was a lower affinity, because the K_i for inhibition for inhibition of substrate uptake was 3-fold higher than that of ATPCA (cf. Fig. 5C and Table 1).

Inhibition of Endogenous Creatine Uptake by Compound 1. Creatine uptake in hippocampal neurons is mediated by CRT-1 (Braissant et al., 2005, Dodd et al., 2010). Thus, we examined the ability of compound **1** (i.e., the inhibitor of CRT-1 with the highest affinity) to inhibit endogenous creatine uptake in these cells. Neuronal cultures were prepared from hippocampi obtained from neonatal rats as described previously (Hotka et al., 2020). The cytosolic ATP/ADP
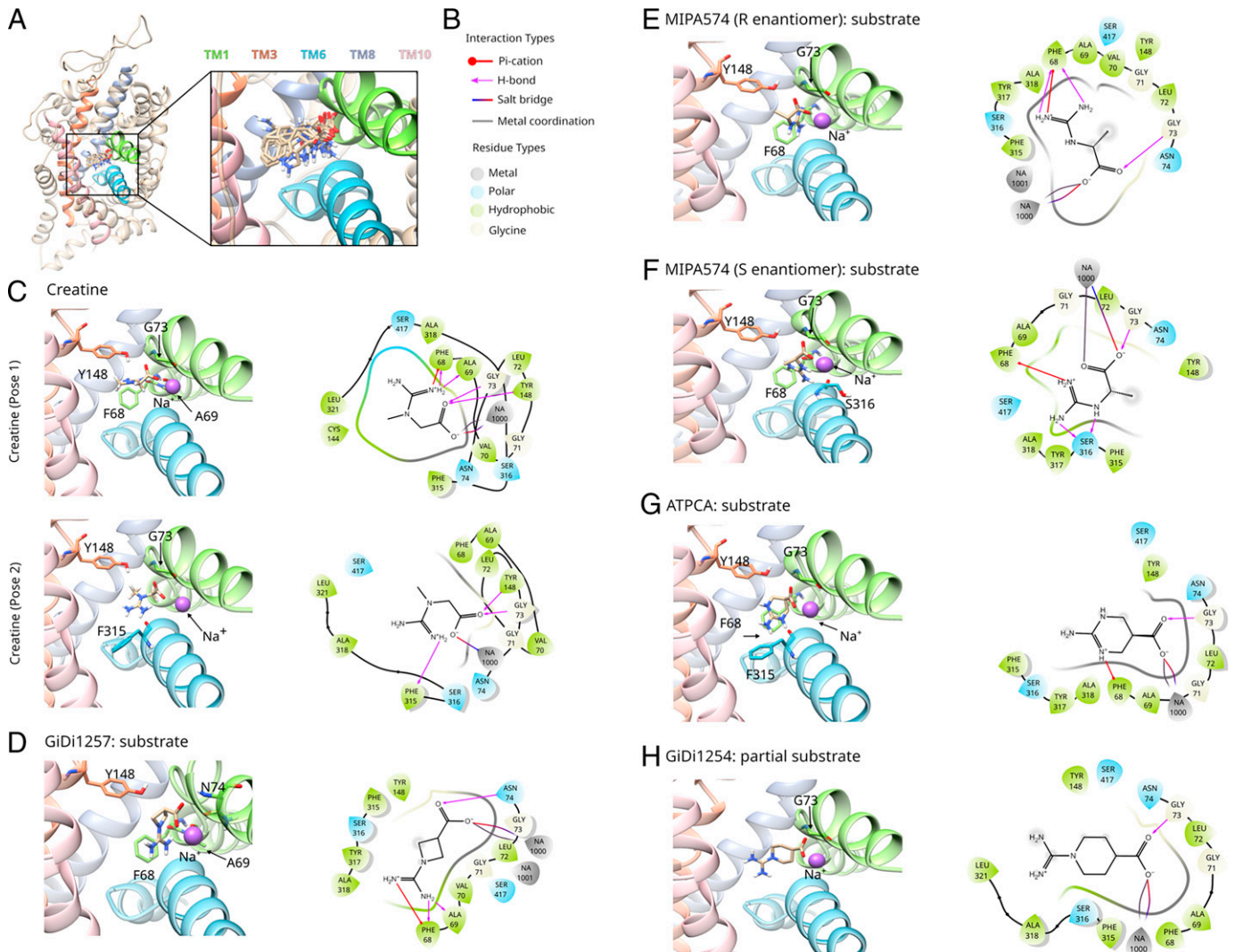
Fig. 3. Interaction of CRT-1 with creatine and the active compounds identified as substrates in present study. (A) The homology model structure of human CRT-1 used for the docking procedure is based on the structure of human SERT (Clarke et al., 2024); the best docked poses of the nine novel compounds are overlaid in the S1 binding site. The ligands are colored in tan (with nitrogens and oxygens in blue and red, respectively). CRT-1 is shown in ribbon representation. The helices are colored in tan, with the exception of the helices lining the S1, which are colored according to the following scheme: TM1 (green), TM3 (orange), TM6 (blue), TM8 (violet), and TM10 (pink). (B) Legend for the ligand interaction diagrams shown in C–H. (C) Docking of creatine into the S1 binding site of CRT-1, as determined by Clarke et al. (2024), shown in a three-dimensional representation (left); the two-dimensional map (right) visualizes the nature of the interactions. Helix coloring is according to the scheme in (A). Clarke et al. (2024) identified two major binding poses for creatine, which are shown here and designated pose 1 (top) and pose 2 (bottom). (D–H) Top docked pose for each of the novel compounds identified as substrates, according to the HADDOCK docking score and distance calculations (see *Methods*). The pose is shown in three dimensions on the left, with the helices colored according to (A) and the ligand colored in tan. Two-dimensional interaction maps are shown on the right. Grey spheres indicate atoms and functional groups on the ligands, which are solvent exposed.

ratio of individual neurons was monitored by the genetically encoded fluorescent indicator PercevalHR, which is comprised of the cyclically permuted green fluorescent protein variant Venus and an optimized variant of the bacterial regulatory protein GnK1, which binds ADP and ATP (Tantama et al., 2013). When excited at 400 to 420 nm, fluorescence emission by PercevalHR is enhanced by ADP; conversely, ATP enhances fluorescence emission after excitation in the range of 480 to 500 nm. Thus, ratiometric fluorescence imaging is independent of the expression levels of PercevalHR (Tantama et al., 2013) and reflects the ATP/ADP ratio. Creatine kinase (reversibly) transfers the γ-phosphate from ATP to creatine to produce ADP and phosphocreatine. Cellular phosphocreatine levels exceed those

of ATP. Hence, under physiological conditions, creatine kinase operates to regenerate ATP from phosphocreatine. Because of the very high catalytic rate of creatine kinase, intracellular phosphocreatine serves as a quasi-instantaneous ATP buffer (Wyss and Kaddurah-Daouk, 2000). We first confirmed that hippocampal neurons rely on the creatine kinase circuit to maintain ATP levels by superfusing neurons with the creatine kinase inhibitor, FDNB (Mahowald et al., 1962; Infante and Davies, 1965). Rapid application of FDNB led to a pronounced decrease in the ATP/ADP-ratio (Fig. 6A). Thus, the DNFB-induced drop in the ATP/ADP-ratio reflected basal cellular ATP consumption, which was not buffered by phosphocreatine due to inhibition of creatine kinase activity.
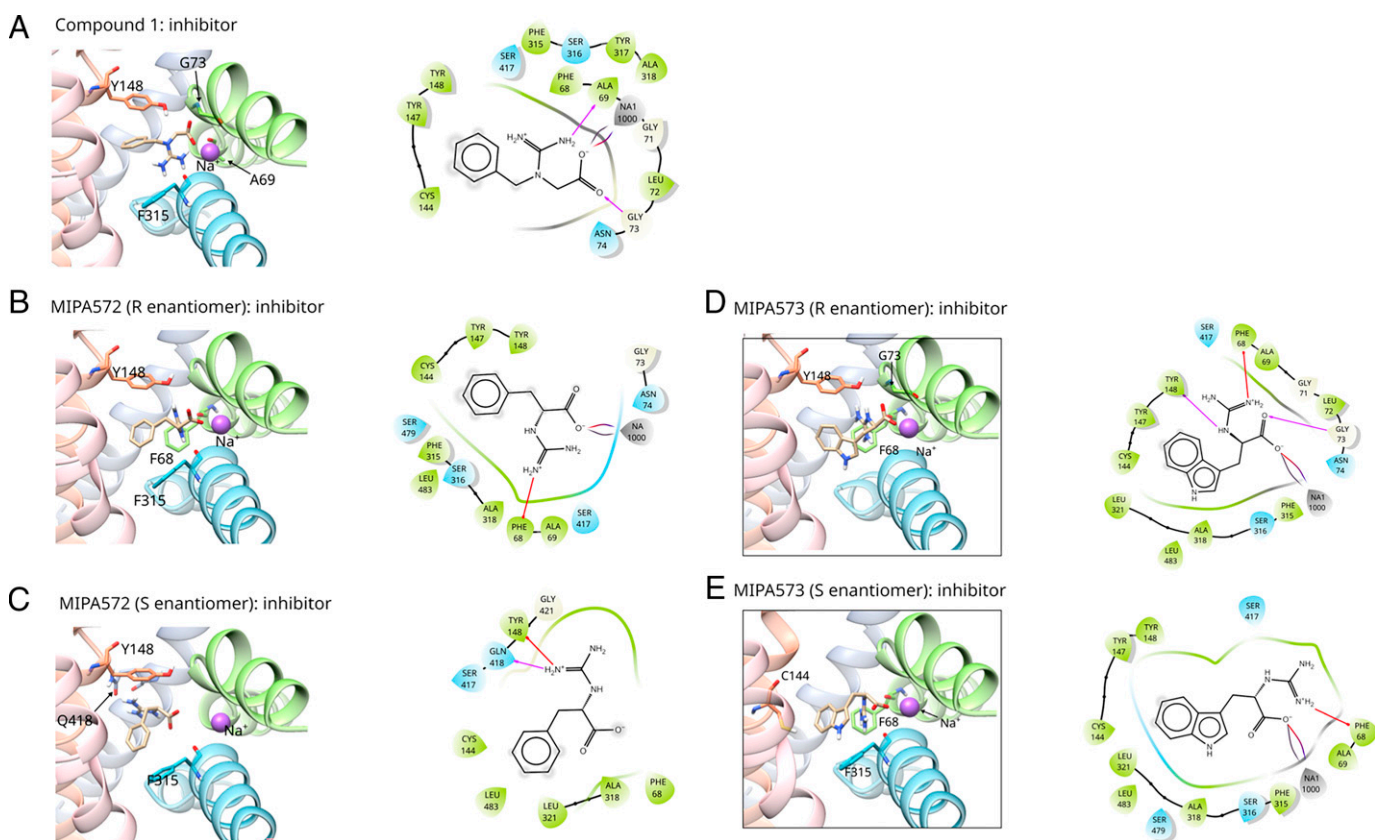
Fig. 4. Interaction of CRT-1 with creatine and the active compounds identified as blockers in the present study. Top docked poses of the three true inhibitors, i.e., compound **1** (A) and the two enantiomers of MIPA572 (B, C) and of MIPA573(D, E). Docking to the SERT-based homology model of CRT-1 was done as outlined in the legend to Fig. 3A and under Materials and Methods. Helices and the ligand interaction diagrams are colored as in Fig. 3.

This observation confirmed that the creatine kinase circuit was operational and that, under the experimental conditions employed, changes in its activity were detectable as alteration of the ATP/ADP ratio because of the high energy demand of neurons. Accordingly, we posited that manipulations of intracellular creatine levels should translate into a prompt change in the ATP/ADP ratio. If this was the case, measuring the ATP/ADP-ratio would allow for monitoring exit or entry of creatine entry into cells in real time. Steady-state levels of intracellular creatine reflect the balance of creatine uptake by CRT-1 and of creatine efflux via the monocarboxylate transporter-12 (Farr et al., 2022). Accordingly, we first monitored the fluorescence response of hippocampal neurons expressing PercevalHR, which were superfused with (creatine-free) buffer in the absence and presence of compound: addition of compound **1** resulted in a readily detectable decline of the ATP/ADP ratio, which proceeded with a rate of approximately 0.5 minutes to reach an equilibrium within 150 seconds (Fig. 6B). The decline was modest, but statistically significant (Fig. 6C). If these neurons were subsequently superfused with 250 μM creatine in the continuous presence of compound **1**, the fluorescence ratio remained constant (blue trace in Fig. 6D). In contrast, in the absence of compound **1**, superfusion of neurons with 250 μM creatine resulted in a prompt decrease in the ATP/ADP ratio, which reached an equilibrium after 400 seconds (black trace in Fig. 6D). Accordingly, a statistically significant decrease in the ATP/ADP ratio was seen, if the fluorometric ratios recorded prior to addition of creatine

were compared with those recorded 400 seconds later only in those neurons which had not been superfused with compound **1** (Fig. 6E). We conclude that, in line with the results from Fig. 1, B and C and Fig. 2B, compound **1** inhibited creatine uptake in living cells.

Discussion

CRT-1 has an impressive concentrative power; its kinetics of substrate and cosubstrate binding have been engineered by evolutionary pressure to maintain the forward transport mode despite progressive accumulation of intracellular substrate (Farr et al., 2022). All available CRT-1 inhibitors (GAA, GPA, GBA, ATPCA, cyclocreatine) are alternative substrates. In fact, our electrophysiological analysis provides formal proof for the conclusion that they are full substrates. Thus, when employed at concentrations which suffice to fully inhibit creatine uptake, they are predicted to reach very high intracellular levels. This prediction has been verified (Fitch et al., 1978). This accumulation limits their application because some of their effects may not arise from inhibition of creatine uptake but from their intracellular accumulation to concentrations in the high millimolar range: GPA (recently renamed ompenaclid) is for instance also a low-efficacy substrate for cytosolic, but not mitochondrial, creatine kinase (Chevli and Fitch, 1979; Oudman et al., 2013). Here, we systematically searched for CRT-1 inhibitors and achieved three key advancements in the pharmacological research of CRT-1:
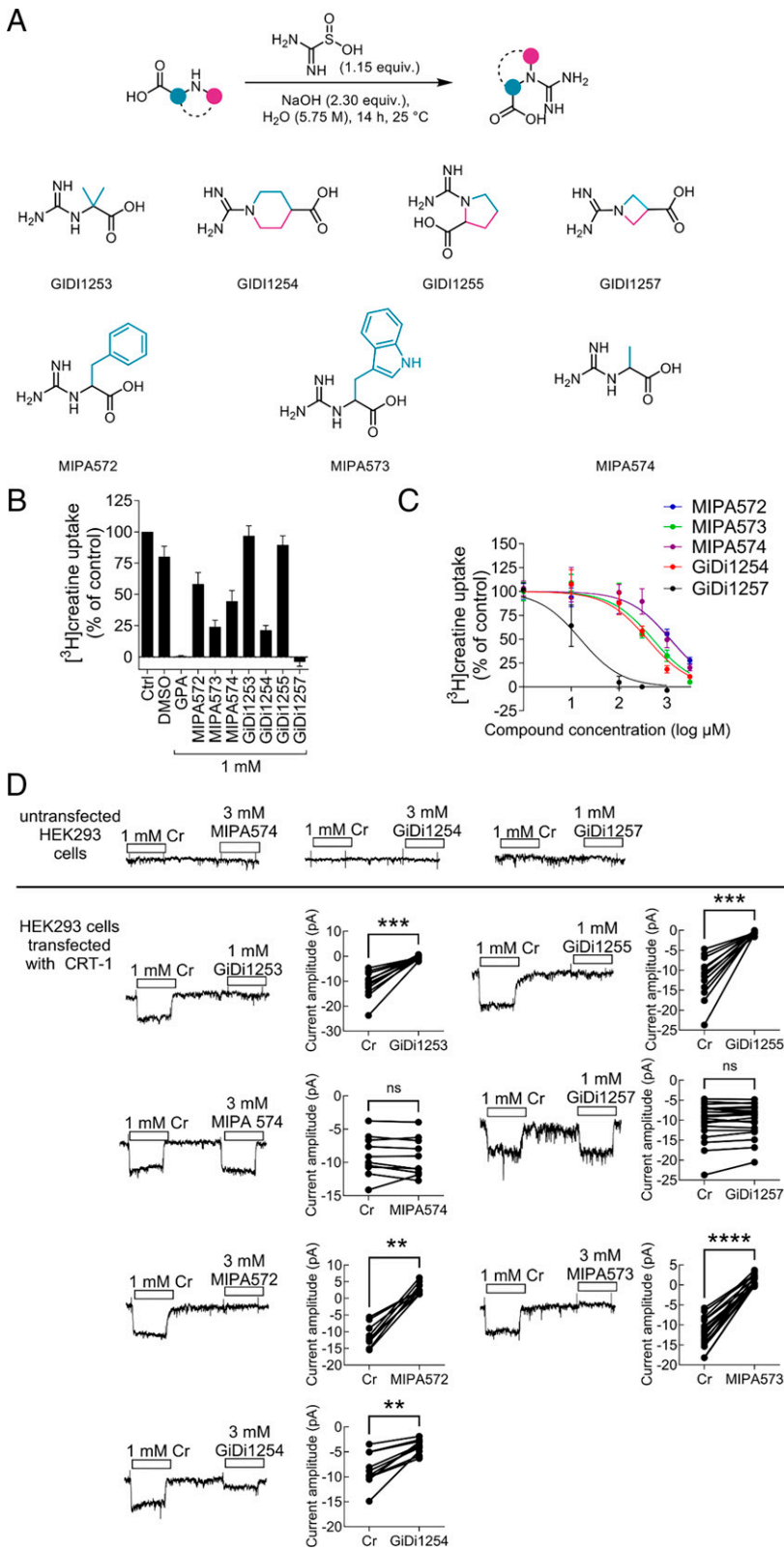
Fig. 5. Schematic representation of the synthesis and structures of the designed and synthesized novel guanidinocarboxylic acids (A) and substrate uptake by (B, C) and transport-associated currents through CRT-1 (D) in the presence of candidate CRT-1 ligands. (A) The synthetic procedures are described in detail under *Materials and Methods*. (B) Inhibition of [³H]creatine uptake into HEK293 cells transiently expressing CRT-1 by the newly synthesized candidate compounds shown in Fig. 3. Specific uptake of [³H]creatine uptake was measured in the absence [buffer control = Ctrl (KRH) and DMSO control = Ctrl (DMSO)] and in the presence of these compounds (1 mM) was divided by the uptake in their absence. Control uptake (Ctrl) amounted to 8.99 ± 1.96 pmol $min^{-1} \cdot 10^{-6}$ cells (standard) and was set to 100% to account for interassay variation. MIPA573 was dissolved in DMSO; as a reference, uptake was also determined in the presence of 2% DMSO to account for carryover (DMSO); this reference amounted to (and 7.29 ± 1.03 pmol min^{-1} 10^{-6} cells. Bars show arithmetic means ± S.D. from four independent experiments. (C) Specific [³H]creatine uptake by HEK293 cells heterologously expressing CRT-1 in the presence of increasing concentrations of MIPA572, MIPA573, MIPA574, GiDi1254 and GiDi1257. Specific [³H]creatine uptake in the presence of (putative) inhibitors was normalized to the uptake in their absence. This control uptake was 7.9 ± 1.8 pmol $min^{-1} \cdot 10^{-6}$ (buffer control) and 6.8 ± 1.5 pmol min^{-1} 10^{-6} (DMSO 2%) and set to 100% to account for interassay variations. The data points were fitted to the equation for a monophasic inhibition curve. The IC$_{50}$ values were estimated as 1.19 ± 0.01 mM, 500 ± 57 μM, 1.15 ± 0.15 mM, 390 ± 93 μM and 14.8 ± 2.4 μM for MIPA572, MIPA573, MIPA574, GiDi1254, and GiDi1257, respectively. Because the concentration of [³H]creatine used in this experiment (0.01 μM) was far below its K$_M$, the IC$_{50}$ values are virtually identical to K$_i$ values. Data are arithmetic means from four independent experiments; error bars indicate S.D. (D) Patch-clamp recordings of transport-associated currents through CRT-1. Currents were recorded in untransfected HEK293 cells and in HEK293 cells transiently expressing CRT-1 in the cell-attached configuration as outlined in Fig. 2A. Cells were first superfused with a saturating concentration (500 μM) of creatine (Cr). Following washout of creatine with external solution, cells were then superfused with saturating concentrations (given above the white boxes, which indicate the superfusion steps) of MIPA572 ($n = 9$), MIPA573 ($n = 19$), MIPA574 ($n = 10$), GiDi1253 ($n = 11$), GiDi1254 ($n = 12$), and GiDi1257 ($n = 21$). Representative traces are shown on the left-hand side for each compound; the right-hand spaghetti plots compare the amplitudes of the steady-state currents recorded in the presence of individual compounds to those elicited by creatine in the same cell. Statistically significant differences were found by the Wilcoxon signed-rank test between creatine and GiDi1253 ($P = 0.001$), GiDi1254 ($P = 0.002$), GiDi1255 (0.0005), MIPA572 ($P = 0.0039$), and MIPA573 ($P < 0.0001$); n.s., not significant, *$P \leq 0.01$; ***$P \leq 0.001$, ****$P \leq 0.0001$.

(i) We extended the pool of CRT-1 ligands by three first-in-class true inhibitors (compound **1**, MIPA572, MIPA573), one partial substrate (GiDi1254) and two novel substrates (GiDi1257, MIPA574). (ii) We demonstrated inhibition of endogenous creatine uptake by one of the newly identified noncompetitive inhibitors. (iii) We inferred structural criteria, which rationally guide the further exploration of the pharmacology of CRT-1.

All transporters of the SLC family operate in a conformational cycle, which allows for alternate access; this requires a
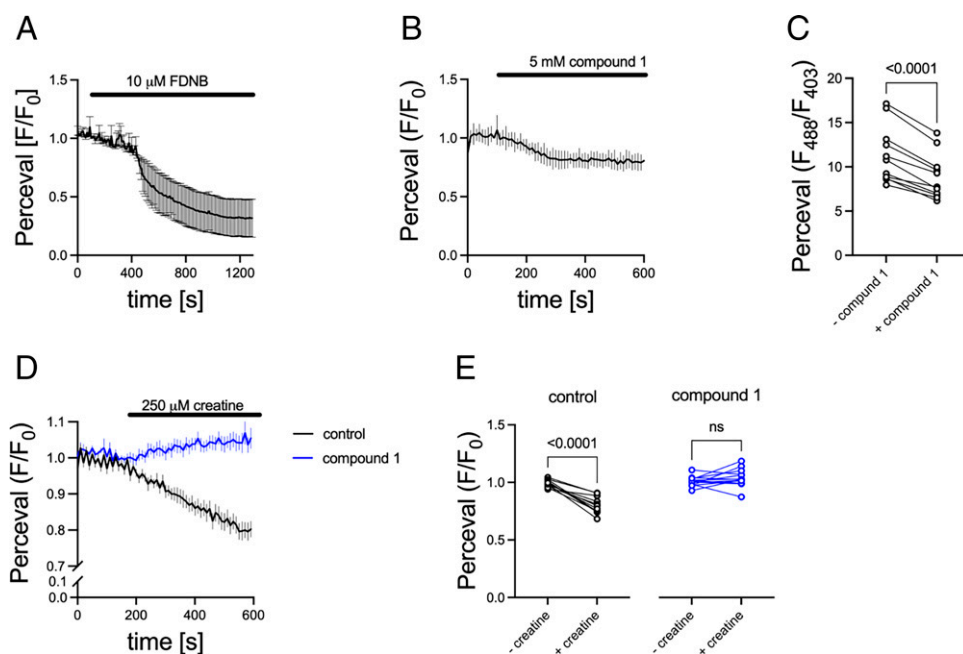
Fig. 6. Inhibition of creatine uptake in hippocampal neurons of neonatal rats by compound 1. Rat hippocampal neurons were transfected with a plasmid encoding the fluorescent protein PercevalHR (referred to as "Perceval"), which allows for monitoring the ratio of cytosolic ATP/ADP by recording fluorescence (F488/F403) emitted at 525 nm after excitation at 488 nm and 403 nm. (A) Change in ATP/ADP ratio induced by superfusion of hippocampal neurons expressing PercevalHR neurons with 10 μM of the creatine kinase inhibitor FDNB: the actual ATP/ADP ratio F was normalized to F_0, i.e., the F488/F403 recorded at time point 0 prior to addition of FDNB (application indicated by black bar). Shown are the means $\pm$ S.D. recorded in independent experiments from three neurons. (B and C) Change in ATP/ADP ratio upon superfusion of hippocampal neurons with compound 1. Neuronal cultures were allowed to equilibrate after removal of the medium by superfusion with (creatine-free) buffer. The ATP/ADP-ratio (F488/F403) of neurons expressing PerecvalHR was recorded for 2 minutes to verify a stable baseline; thereafter, superfusion with compound 1 (5 mM) was initiated and the ATP/ADP-ratio (F488/F403) was continuously recorded. Data are means $\pm$ S.D. recorded in independent experiments from 11 neurons. The actual ATP/ADP ratio F was normalized to F_0 as in panel A. The spaghetti plot in panel C summarizes the F488/F403 ratio for each individual neuron recorded prior to addition of compound 1 (-compound 1) and after 400 seconds of superfusion with compound 1 (+compound 1). The difference was statistically significant (paired t test, $P = 0.0088$; ***$P \leq 0.01$). (D and E) Change in ATP/ADP-ratio of hippocampal neurons superfused with 250 μM creatine in the absence and presence of 5 mM compound 1. Neurons were first superfused for 8 minutes in the absence and presence of compound 1 (5 mM) as shown in panel C to reach a stable baseline fluorescence ratio (the last 200 seconds of this equilibration period are shown). Thereafter, the superfusion with 250 μM creatine (indicated by black bar) was initiated in the absence (black trace) and continuous presence of 5 mM compound 1 (blue trace, Com1). The F488/F403 ratio was normalized as in panel A to the F488/F403 ratio recorded at time point 0 ("F0", i.e., prior to the start of the superfusion with creatine). Sown are the means $\pm$ S.D. recorded in independent experiments from 11 and 12 neurons in the absence and presence of compound 1, respectively. In pane E, the initial ATP/ADP-ratio, i.e., prior to addition of creatine, and the ATP/ADP-ratio after 600 seconds was plotted for each individual neuron imaged in panel D (- creatine = time point 0; + creatine = time point 400 seconds later). A statistically significant difference was only seen in the absence of compound 1 (paired t test, $P = 0.001$; ****; n.s., not significant).

minimum of three conformations, an outward-facing open state, an occluded state, and an inward-facing open state, to translocate substrate across the cell membrane (Drew and Boudker, 2016). In the extracellularly-facing open state of eukaryotic SLC6 transporters, the substrate molecule is accommodated together with sodium and chloride (except for the chloride-independent SLC6A15, SLC6A17, SLC6A19) in a binding site present in the center of the water-accessible pathway; this binding site is referred to as the S1. The serotonin transporter and the other monoamine transporters also harbor a vestibular binding site, referred to as an S2-site, which can be targeted by allosteric ligands (Zhu et al., 2016; Plenge et al., 2021; El-Kasaby et al., 2024). At present, it is not clear, if a vestibular binding site is also present in CRT-1. In fact, there are several distinct binding sites within the vestibule of three monoamine transporters of the SLC6 family (Supplemental Fig. 2). Only compounds simultaneously harboring a carboxyl- and guanidino-group inhibited CRT-1-mediated [3H]creatine translocation. This is consistent with earlier investigations (see Supplemental Tables 1 and 2). Due to the structural similarity of these compounds with

creatine, we infer that they bound to the S1-site (i.e., they are orthosteric ligands). The requirement of the simultaneous presence of a carboxyl and guanidino group indicates that either group interacts with opposite residues within S1. Indeed, computational studies indicated that the carboxyl-group interacted with Gly73 and Tyr148, while the guanidino-group interacted with Phe68 (docking pose 1 in Fig. 3C) or Phe315 (docking pose 2 in Fig. 3C) (Clarke et al., 2024). Consistent with this assignment, Phe68 was identified as a major determinant of ligand selectivity of CRT-1: combinations of two to three amino acid substitutions convert CRT-1 to a GABA transporter; all but one of the required combined mutations included Phe68 (Dodd and Christie, 2007). GABA is not transported by CRT-1 and differs from GPA by the absence of two nitrogen atoms, highlighting the role of the guanidino group in binding to CRT-1. The importance of an unaltered guanidino-group for recognition by CRT-1 is reinforced by two further observations: (i) Disruption of the delocalized electron system as found in the guanidino-group by additional nitrogen atoms (compounds 3 and 8) precluded binding to CRT-1. (ii) Removal of a nitrogen atom converts ATPCA to ATPCA II,

which has a 10-fold lower affinity than ATCPA (Al-Khawaja et al., 2018).

Apart from Gly73 and Tyr148, the carboxyl-group is predicted to electrostatically interact with a sodium ion, i.e., Na$^+$1 (Fig. 3C) (Clarke et al., 2024, Colas et al., 2020). We suspect that this charge interaction fails to form with guanidinocarboxylic acids harboring additional charges (compounds **5** and **7**; guanidinosuccinate) explaining their inability to block CRT-1. GiDi1255 has the defining features of a substrate, i.e., a guanidino-group separated by one carbon atom from the carboxylate-group, but their mobility is restrained to place them in an acute angle. GiDi1255 was neither a substrate nor an inhibitor of CRT-1. This indicates that the simultaneous presence of the carboxylate- and the guanidino-group does not suffice per se: binding to CRT-1 is contingent on an extended conformation, which supports the π-interaction of the guanidino-group with Phe68 (Fig. 3C). This interpretation is supported by molecular dynamics simulations (Clarke et al., 2024) and by the observation that GiDi1257 was a high-affinity substrate of CRT-1 (Fig. 2D). The fact that the affinity of GiDi1257 exceeded that of the cognate substrate and of all other known substrates shows that a reduction in flexibility is not an impediment to binding.

The transmembrane helices of SLC6 carriers can be divided into a scaffold and a bundle domain. Substrate translocation occurs through rocking of the bundle domain against the fixed scaffold domain and is preceded by occlusion of the outer gate of the transporter (Forrest et al., 2008). According to the "hold-and-pull" model of SERT, interactions between the ligand and residues in both the bundle and scaffold domain are required for inducing occlusion (Gradisch et al., 2022): via its indole moiety, serotonin is held in place, allowing the ethylamine moiety of serotonin to pull the bundle domain toward the scaffold domain, permitting closure of the outer gate. Clarke et al. (2024) proposed that a similar mechanism triggers occlusion in CRT-1: Y148 (in the scaffold domain) holds the carboxyl-group of creatine in a fixed position, while a sodium ion (coordinated by residues of the bundle domain) exerts an attractive force on creatine. Given that they harbor a carboxyl-group, we suspect that, after having bound via the combined action of the guanidino and carboxylate group, previously known substrates (creatine, GAA, GPA, GBA, cyclocreatine, ATPCA) and novel substrates (GiDi1254, GiDi1257, MIPA574) of CRT-1 induce occlusion via this mechanism. Partial substrates are compounds which are transported at lower rates than full substrates (Rothman et al., 2012). In SERT, a continuum extends from full over partial substrates to inhibitors, which is, at least in part, determined by steric bulk (Sandtner at al., 2016, Bhat et al., 2017). GiDi1254 constitutes the first identified partial CRT-1 substrate. Submaximal transport rates may arise from deceleration of any step in the transport cycle. All full substrates, which we docked (creatine, GiDi1254, MIPA574, ATPCA), form a π-interaction with Phe68 (Fig. 3, B–H). This interaction is absent in the most prevalent docking pose of the partial substrate GiDi1257 (Fig. 3G), presumably precluded by its bulky ring.

Addition of neutral bulk to guanidinocarboxylic acids as represented by compound **1**, MIPA572, and MIPA573 did not preclude their inhibiting and thus binding to CRT-1. Therefore, it is more likely that the enlarged bulk present in GiDi1254 causes partial efficacy by hampering occlusion.

Consequently, we suspect that the neutral bulk present in the linker region of compound **1**, MIPA572, and MIPA573 blocks occlusion fully by steric hindrance. This conjecture is supported by the results from molecular docking (Fig. 4, A–E).

Elimination of the methyl group of creatine yields GAA and halves the affinity to CRT-1. The methyl group confers affinity by a hydrophobic interaction with Cys144 (pose 1, Fig. 3A). The affinity of MIPA574 was decreased when compared with creatine. Slight repositioning of the methyl group as represented by MIPA574 results in the loss of interaction with the hydrophobic pocket, regardless of which enantiomer is examined (Fig. 3, E–F). In addition, the methyl group may affect affinity via a positive inductive effect on the guanidino group (i.e., by increasing the positive charge of the guanidino-group). This model may also explain why compound **1**, which carries the neutral bulk on the nitrogen atom which is methylated in creatine, has a higher affinity to CRT-1 than MIPA572 and MIPA573 (which are substituted on the linker region).

Many CRT-1 mutants associated with the creatine transporter deficiency syndrome are folding-deficient (El-Kasaby et al., 2019). Folding deficiencies can be corrected by indirect modulation of the folding process (chemical chaperones) or via specific binding to the misfolded protein (pharmacochaperones) (Freissmuth et al., 2018). Indeed, chemical chaperoning rescues some creatine transporter deficiency-associated CRT-1 mutants (El-Kasaby et al., 2019). Given this proof-of-principle, pharmacochaperones of CRT-1 are desirable, because there are no any alternative treatment strategies for CTD. Pharmacochaperones remedy the folding deficiency by stabilizing unique conformational states in the folding trajectory (Freissmuth et al., 2018). Full substrates trigger the transport cycle, i.e., the transporter visits many different states. Accordingly, they do not act as pharmacochaperones (Bhat et al., 2019). Partial substrates, however, preclude rapid transitions by stabilizing conformational intermediates. Indeed, partial substrates rescue folding-deficient SERT and DAT variants (Bhat et al., 2017, 2020). Therefore, the identification of a partial substrate of CRT-1 is a starting point in the search for pharmacochaperones acting on CRT-1 mutants.

Data Availability

The authors declare that all the data supporting the findings of this study are contained within the paper.

Authorship Contributions

Participated in research design: Farr, Sandtner, Stockner, Klade, Maulide, Freissmuth.

Conducted experiments: Farr, El-Kasaby, Hotka, Clarke.

Contributed new reagents or analytic tools: Xiao, Schupp, DiMauro, Pastor Fernandez.

Performed data analysis: Farr, Xiao, El-Kasaby, Hotka, Sandtner, Stockner, Maulide, Freissmuth.

Wrote or contributed to the writing of the manuscript: Farr, Hotka, Clarke, Sandtner, Stockner, Maulide, Freissmuth.

References

Al-Khawaja A, Haugaard AS, Marek A, Löffler R, Thiesen L, Santiveri M, Damgaard M, Bundgaard C, Frølund B, and Wellendorph P (2018) Pharmacological Characterization of [³H]ATPCA as a Substrate for Studying the Functional Role of the Betaine/GABA Transporter 1 and the Creatine Transporter. *ACS Chem Neurosci* 9:545–554.

Asjad HMM, Kasture A, El-Kasaby A, Sackel M, Hummel T, Freissmuth M, and Sucic S (2017) Pharmacochaperoning in a drosophila model system rescues human dopamine transporter variants associated with infantile/juvenile parkinsonism. *J Biol Chem* 292:19250–19265.

Bhat S, Hasenhuetl PS, Kasture A, El-Kasaby A, Baumann MH, Blough BE, Sucic S, Sandtner W, and Freissmuth M (2017) Conformational state interactions provide clues to the pharmacochaperone potential of serotonin transporter partial substrates. *J Biol Chem* 292:16773–16786.

Bhat S, Newman AH, and Freissmuth M (2019) How to rescue misfolded SERT, DAT and NET: targeting conformational intermediates with atypical inhibitors and partial releasers. *Biochem Soc Trans* 47:861–874.

Bhat S, Guthrie DA, Kasture A, El-Kasaby A, Cao J, Bonifazi A, Ku T, Giancola JB, Hummel T, Freissmuth M, et al. (2020) Tropane-Based Ibogaine Analog Rescues Folding-Deficient Serotonin and Dopamine Transporters. *ACS Pharmacol Transl Sci* 4:503–516.

Bhat S, El-Kasaby A, Fischer FP, Freissmuth M, and Sucic S (2021) Functional and biochemical consequences of disease variants in neurotransmitter transporters: a special emphasis on folding and trafficking deficits. *PharmacolTher* 222:107785.

Bhat S, El-Kasaby A, Kasture A, Boytsov D, Reichelt JB, Hummel T, Sucic S, Pifl C, Freissmuth M, and Sandtner W (2023) A mechanism of uncompetitive inhibition of the serotonin transporter. *Elife* 12:e82641.

Beerepoot P, Lam VM, and Salahpour A (2016) Pharmacological Chaperones of the Dopamine Transporter Rescue Dopamine Transporter Deficiency Syndrome Mutations in Heterologous Cells. *J Biol Chem* 291:22053–22062.

Braissant O, Henry H, Villard A-M, Speer O, Wallimann T, and Bachmann C (2005) Creatine synthesis and transport during rat embryogenesis: spatiotemporal expression of AGAT, GAMT and CT1. *BMC Dev Biol* 5:9.

Bulling S, Schicker K, Zhang Y-W, Steinkellner T, Stockner T, Gruber CW, Boehm S, Freissmuth M, Rudnick G, Sitte HH, et al. (2012) The mechanistic basis for noncompetitive ibogaine inhibition of serotonin and dopamine transporters. *J Biol Chem* 287:18524–18534.

Casiraghi A, Bensimon A, and Superti-Furga G (2021) Recent developments in ligands and chemical probes targeting solute carrier transporters. *Curr Opin Chem Biol* 62:53–63.

César-Razquin A, Snijder B, Frappier-Brinton T, Isserlin R, Gyimesi G, Bai X, Reithmeier RA, Hepworth D, Hediger MA, Edwards AM, et al. (2015) A Call for Systematic Research on Solute Carriers. *Cell* 162:478–487.

Chevli R and Fitch CD (1979) β-Guanidinopropionate and phosphorylated β-guanidinopropionate as substrates for creatine kinase. *Biochem Med* 21:162–167.

Chiba P, Freissmuth M, and Stockner T (2014) Defining the blanks - pharmacochaperoning of SLC6 transporters and ABC transporters. *Pharmacol Res* 83:63–73.

Clarke A, Farr CV, El-Kasaby A, Szöllősi D, Freissmuth M, Sucic S, and Stockner T (2024) Probing binding and occlusion of substrate in the human creatine transporter-1 by computation and mutagenesis. *Protein Sci* 33:e4842.

Colas C, Banci G, Martini R, and Ecker GF (2020) Studies of structural determinants of substrate binding in the Creatine Transporter (CreaT, SLC6A8) using molecular models. *Sci Rep* 10:6241.

Dai W, Vinnakota S, Qian X, Kunze DL, and Sarkar HK (1999) Molecular characterization of the human CRT-1 creatine transporter expressed in Xenopus oocytes. *Arch Biochem Biophys* 361:75–84.

de la Rocha-Muñoz A, Melgarejo E, Aragón C, and López-Corcuera B (2021) Rescue of two trafficking-defective variants of the neuronal glycine transporter GlyT2 associated to hyperekplexia. *Neuropharmacology* 189:108543.

Dodd JR, Birch NP, Waldvogel HJ, and Christie DL (2010) Functional and immunocytochemical characterization of the creatine transporter in hippocampal neurons. *J Neurochem* 115:684–693.

Dodd JR and Christie DL (2007) Selective amino acid substitutions convert the creatine transporter to a γ-aminobutyric acid transporter. *J Biol Chem* 282:15528–15533.

Drew D and Boudker O (2016) Shared Molecular Mechanisms of Membrane Transporters. *Annu Rev Biochem* 85:543–572.

El-Kasaby A, Just H, Malle E, Stolt-Bergner PC, Sitte HH, Freissmuth M, and Kudlacek O (2010) Mutations in the carboxyl-terminal SEC24 binding motif of the serotonin transporter impair folding of the transporter. *J Biol Chem* 285:39201–39210.

El-Kasaby A, Kasture A, Koban F, Hotka M, Asjad HMM, Kubista H, Freissmuth M, and Sucic S (2019) Rescue by 4-phenylbutyrate of several misfolded creatine transporter-1 variants linked to the creatine transporter deficiency syndrome. *Neuropharmacology* 161:107572. 2019,

El-Kasaby A, Boytsov D, Kasture A, Krumpl G, Hummel T, Freissmuth M, and Sandtner W (2024) Allosteric Inhibition and Pharmacochaperoning of the Serotonin Transporter by the Antidepressant Drugs Trazodone and Nefazodone. *Mol Pharmacol* 106:56–70.

Farr CV, El-Kasaby A, Freissmuth M, and Sucic S (2020) The Creatine Transporter Unfolded: A Knotty Premise in the Cerebral Creatine Deficiency Syndrome. *Front Synaptic Neurosci* 12:588954.

Farr CV, El-Kasaby A, Erdem FA, Sucic S, Freissmuth M, and Sandtner W (2022) Cooperative Binding of Substrate and Ions Drives Forward Cycling of the Human Creatine Transporter-1. *Front Physiol* 13:919439.

Fitch CD, Shields RP, Payne WF, and Dacus JM (1968) Creatine Metabolism in Skeletal Muscle III. Specificity of the Creatine Entry Process. *J Biol Chem* 243:2024–2027.

Fitch CD, Chevli R, Petrofsky JS, and Kopp SJ (1978) Sustained isometric contraction of skeletal muscle depleted of phosphocreatine. *Life Sci* 23:1285–1291.

Forrest LR, Zhang Y-W, Jacobs MT, Gesmonde J, Xie L, Honig BH, and Rudnick G (2008) Mechanism for alternating access in neurotransmitter transporters. *Proc Natl Acad Sci U S A* 105:10338–10343.

Freissmuth M, Stockner T, and Sucic S (2018) SLC6 Transporter Folding Diseases and Pharmacochaperoning. *Handb Exp Pharmacol* 245:249–270.

Gradisch R, Szöllősi D, Niello M, Lazzarin E, Sitte HH, and Stockner T (2022) Occlusion of the human serotonin transporter is mediated by serotonin-induced conformational changes in the bundle domain. *J Biol Chem* 298:101613.

Hasenhuetl PS, Bhat S, Freissmuth M, and Sandtner W (2019) Functional Selectivity and Partial Efficacy at the Monoamine Transporters: A Unified Model of Allosteric Modulation and Amphetamine-Induced Substrate Release. *Mol Pharmacol* 95:303–312.

Hotka M, Cagalinec M, Hilber K, Hool L, Boehm S, and Kubista H (2020) L-type Ca²⁺ channel-mediated Ca²⁺ influx adjusts neuronal mitochondrial function to physiological and pathophysiological conditions. *Sci Signal* 13:eaaw6923.

Honorato RV, Koukos PI, Jiménez-García B, Tsaregorodtsev A, Verlato M, Giachetti A, Rosato A, and Bonvin AMJJ (2021) Structural Biology in the Clouds: the WeNMR-EOSC Ecosystem. *Front Mol Biosci* 8:729513.

Infante AA and Davies RE (1965) The effect of 2,4-dinitrofluorobenzene on the activity of striated muscle. *J Biol Chem* 240:3996–4001.

Jacobs MT, Zhang Y-W, Campbell SD, and Rudnick G (2007) Ibogaine, a noncompetitive inhibitor of serotonin transport, acts by stabilizing the cytoplasm-facing state of the transporter. *J Biol Chem* 282:29441–29447. 2007,

Jursic BS, Neumann D, and McPherson A (2000) Preparation of N-formamidinylamino acids from amino and formamidinesulfinic acid. *Synthesis 2000* 12:1656–1658. DOI: 10.1055/s-2000-8201

Kasture A, El-Kasaby A, Szöllősi D, Asjad HMM, Grimm A, Stockner T, Hummel T, Freissmuth M, and Sucic S (2016) Functional Rescue of a Misfolded Drosophila Melanogaster Dopamine Transporter Mutant Associated with a Sleepless Phenotype by Pharmacological Chaperones. *J Biol Chem* 291:20876–20890.

Kasture AS, Fischer FP, Kunert L, Burger ML, Burgstaller AC, El-Kasaby ALI, Hummel T, and Sucic S (2022) Drosophila melanogaster as a model for unraveling unique molecular features of epilepsy elicited by human GABA transporter 1 variants. *Front Neurosci* 16:1074427

Ku CP and Passow H (1980) Creatine and creatinine transport in old and young human red blood cells. *Biochim Biophys Acta* 600:212–227.

Kurth J, Yamaguchi N, Andreu-Agullo C, Tian HS, Sridhar S, Takeda S, Gonsalves FC, Loo JM, Barlas A, Manova-Todorova K, et al. (2021) Therapeutic targeting of SLC6A8 creatine transporter suppresses colon cancer progression and modulates human creatine levels. *Sci Adv* 7:eabi7511.

Lygate CA, Lake HA, McAndrew DJ, Neubauer S, and Zervou S (2022) Influence of homoarginine on creatine accumulation and biosynthesis in the mouse. Influence of homoarginine on creatine accumulation and biosynthesis in the mouse. *Front Nutr* 9:969702.

Mahowald TA, Noltmann EA, and Kuby SA (1962) Studies on adenosine triphosphate transphosphorylases. III. Inhibition reactions. *J Biol Chem* 237:1535–1548.

Möller A and Hamprecht B (1989) Creatine transport in cultured cells of rat and mouse brain. *J Neurochem* 52:544–550.

Niello M, Gradisch R, Loland CJ, Stockner T, and Sitte HH (2020) Allosteric Modulation of Neurotransmitter Transporters as a Therapeutic Strategy. *Trends Pharmacol Sci* 41:446–463.

Oudman I, Clark JF, and Brewster LM (2013) The effect of the creatine analogue β-guanidinopropionic acid on energy metabolism: a systematic review. *PLoS One* 8:e52879.

Plenge P, Yang D, Salomon K, Laursen L, Kalenderoglou IE, Newman AH, Gouaux E, Coleman JA, and Loland CJ (2021) The antidepressant drug vilazodone is an allosteric inhibitor of the serotonin transporter. *Nat Commun* 12:5063.

Rothman RB, Partilla JS, Baumann MH, Lightfoot-Siordia C, and Blough BE (2012) Studies of the biogenic amine transporters. 14. Identification of low-efficacy "partial" substrates for the biogenic amine transporters. *J Pharmacol Exp Ther* 341:251–262.

Sandtner W, Stockner T, Hasenhuetl PS, Partilla JS, Seddik A, Zhang Y-W, Cao J, Holy M, Steinkellner T, Rudnick G, et al. (2016) Binding Mode Selection Determines the Action of Ecstasy Homologs at Monoamine Transporters. *Mol Pharmacol* 89:165–175.

Schloss P, Mayser W, and Betz H (1994) The putative rat choline transporter CHOT1 transports creatine and is highly expressed in neural and muscle-rich tissues. *Biochem Biophys Res Commun* 198:637–645.

Sitte HH and Freissmuth M (2015) Amphetamines, new psychoactive drugs and the monoamine transporter cycle. *Trends Pharmacol Sci* 36:41–50.

Stary D and Bajda M (2023) Taurine and Creatine Transporters as Potential Drug Targets in Cancer Therapy. *Int J Mol Sci* 24:3788.

Tachikawa M, Fujinawa J, Takahashi M, Kasai Y, Fukaya M, Sakai K, Yamazaki M, Tomi M, Watanabe M, Sakimura K, et al. (2008) Expression and possible role of creatine transporter in the brain and at the blood-cerebrospinal fluid barrier as a transporting protein of guanidinoacetate, an endogenous convulsant. *J Neurochem* 107:768–778.

Tantama M, Martínez-François JR, Mongeon R, and Yellen G (2013) Imaging energy status in live cells with a fluorescent biosensor of the intracellular ATP-to-ADP ratio. *Nat Commun* 4:2550.

Valayannopoulos V, Bakouh N, Mazzuca M, Nonnenmacher L, Hubert L, Makaci F-L, Chabli A, Salomons GS, Mellot-Draznieks C, Brulé E, et al. (2013) Functional and electrophysiological characterization of four non-truncating mutations responsible for creatine transporter (SLC6A8) deficiency syndrome. *J Inherit Metab Dis* 36:103–112.

van de Kamp JM, Betsalel OT, Mercimek-Mahmutoglu S, Abulhoul L, Grünewald S, Anselm I, Azzouz H, Bratkovic D, de Brouwer A, Hamel B, et al. (2013) Phenotype

and genotype in 101 males with X-linked creatine transporter deficiency. *J Med Genet* **50**:463–472.

van Zundert GCP, Rodrigues JPGLM, Trellet M, Schmitz C, Kastritis PL, Karaca E, Melquiond ASJ, van Dijk M, de Vries SJ, and Bonvin AMJJ (2016) The HAD-DOCK2.2 Web Server: User-Friendly Integrative Modeling of Biomolecular Complexes. *J Mol Biol* **428**:720–725.

van der Kolk MR, Janssen MACH, Rutjes FPJT, and Blanco-Ania D (2022) Cyclobutanes in Small-Molecule Drug Candidates. *ChemMedChem* **17**:e202200020.

Wang WW, Gallo L, Jadhav A, Hawkins R, and Parker CG (2020) The Druggability of Solute Carriers. *J Med Chem* **63**:3834–3867.

Wyss M and Kaddurah-Daouk R (2000) Creatine and creatinine metabolism. *Physiol Rev* **80**:1107–1213.

Zhu R, Sinwel D, Hasenhuetl PS, Saha K, Kumar V, Zhang P, Rankl C, Holy M, Sucic S, Kudlacek O, et al. (2016) Nanopharmacological Force Sensing to Reveal Allosteric Coupling in Transporter Binding Sites. *Angew Chem Int Ed Engl* **55**:1719–1722.

Address correspondence to: Michael Freissmuth, Institute of Pharmacology and the Gaston H. Glock Research Laboratories for Exploratory Drug Development, Center of Physiology and Pharmacology, Medical University of Vienna, Vienna, Waehringerstrasse 13a, Vienna, 1090 Austria. E-mail: michael.freissmuth@meduniwien.ac.at